AD NUMBER

AD800055

NEW LIMITATION CHANGE

TO

Approved for public release, distribution unlimited

FROM

Distribution authorized to U.S. Gov't. agencies and their contractors; Administrative/Operational use; 29 Sep 1966. Other requests shall be referred to AFRPL[RPPR-STINFO], Edwards, California 93523.

AUTHORITY

AFRPL ltr, 20 Dec 1971

DOWNEY PLANT

RESEARCH DIVISION

PROJECT SOPHY

SOLID PROPELLANT HAZARDS PROGRAM

Technical Documentary Report No.
AFRPL-TR-66-26

Progress Report On
Contract AF 04(611)-10919

Report Number 0977-01(04)QP / September 1966 / Copy 77

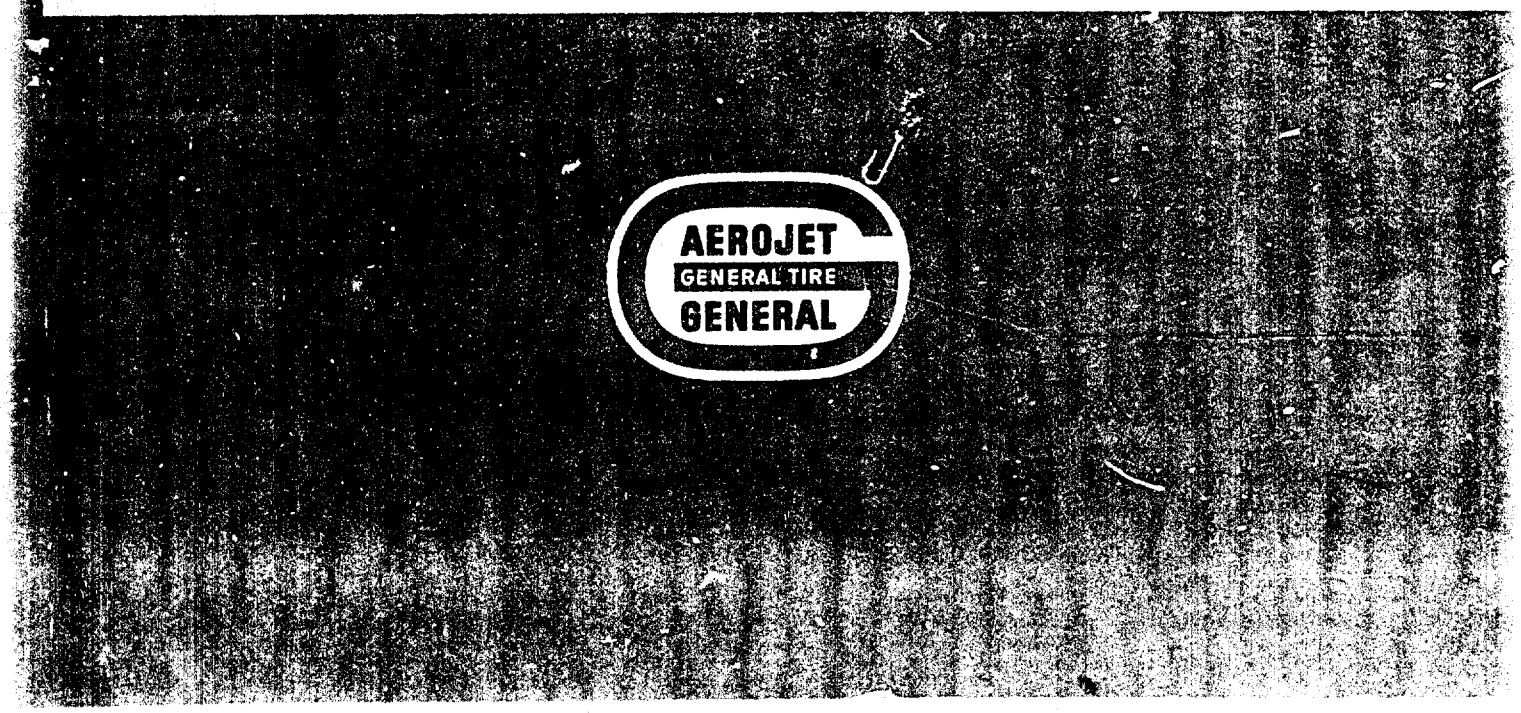

AEROJET-GENERAL CORPORATION
Research Division
11711 Woodruff Avenue
Downey, California

PROGRESS REPORT

PROJECT SOPHY

SOLID PROPELLANT HAZARDS PROGRAM

Technical Documentary Report No.
AFRPL-TR-66-26

Contract AF 04(611)-10919

0977-01(04)QP

Period Covered: 1 June - 31 August 1966

Prepared by: R. B. Elwell
O. R. Irwin
R. W. Vail, Jr.

Date: 29 September 1966

Reviewed by: M. Nishibayashi
M. Nishibayashi, Head
Explosive Kinetics Dept

No. of Pages: 93

Approved by: H. W. Fisher
H. W. Fisher, Manager
Research Division

Classification: UNCLASSIFIED

CONTENTS

ILLUSTRATIONS

ILLUSTRATIONS (Cont.)

TABLES

TABLES (Cont.)

1. INTRODUCTION

This quarterly progress report is the fourth of a series partially fulfilling Contract AF04(611)10919, Large Solid-Propellant Boosters Explosives Hazards Study Program. The purpose of this program is to gain additional knowledge, and to develop new techniques, for analyzing the explosives hazard and damage potential of large solid-propellant rocket motors.

The objectives of this program are: (1) to determine the influence of grain shape on propellant detonability and sensitivity, (2) to determine the critical diameter of a typical solid composite rocket-motor propellant, (3) to determine what changes a solid-propellant grain might undergo when exposed to operational mishaps, and (4) to developmethods to simulate and characterize these alterations.

2. SUMMARY

The mean critical diameter of AAB-3189, an AP-PBAN propellant adulterated with 9.2 weight percent RDX, has been determined to be 2.66 in. The standard deviation of the data is 0.04 in. The mean critical geometry of AAB-3189 in the square cross-section shape is 2.49 in., with a standard deviation of 0.04 in.

The mean critical diameter of AAB-3225 (7.1 weight percent RDX) has been determined for each of three batches. Analysis of the mixing and casting records has not provided an explanation for the large difference between the critical diameter of Batch 4EH-84 material (6.36 in.) and the critical diameters obtained from Batch 4EH-44 and Batch 4EH-107 samples (5.22 and 5.24 in.). The standard deviation in the data from any one batch was no greater than 0.07 in.

Detonation velocities have been measured in circular-cylindrical and square-column shapes, in from near-critical to near-ideal sizes. The samples, composed of AAB-3189 adulterated propellant, were instrumented to obtain reaction-zone thickness data. Analysis of the data from these tests is being performed to determine whether solid propellant behaves according to a Jones-type detonation model.

Samples have been cast for the jetting phenomena study. They consist of a series of hollow-core circular cylinders with inner diameters of various sizes.

Molds have been fabricated, and casting scheduled, for the critical-geometry tests of triangular, rectangular, and hollow-core shaped samples of AAB-3189. Supercritical samples of AAB-3225 are also ready to be cast for use in conventional card-gap sensitivity tests.

Axial resistance probes are being designed for use in the investigation of the sensitivity to initiation of detonation of unadulterated propellant.

The critical-diameter test of a 60-in.-diameter cylindrical sample of unadulterated AP-PBAN (ANB-3226) resulted in failure of the propellant to sustain detonation. The NO-GO test result agrees with the prediction of the theoretical model that has been developed under the SOPHY program.

The testing of an 84-in. diameter sample, in the large critical-diameter task, has been cancelled to allow redirection of technical effort toward an expanded study of the sensitivity of the detonable unadulterated propellant. Official acceptance of the proposed substitute program presently is being sought.

The experimental program to prepare propellant samples containing controlled defects has succeeded in isolating the parameters most effective in determining (unconnected) pore sizes and distributions. Efforts are being made to evaluate analytical methods by which the porous propellant can be characterized.

3. TECHNICAL DISCUSSION

3.1 DEVELOPMENT OF DATA ANALYSIS TECHNIQUES

During this period two techniques have been in the process of development that will assist in the analysis of detonation velocity (D) vs reduced distance (x/d) data obtained from critical-geometry test records. In one, the raw distance-time data is put into a computer program that calculates and prints out D vs x/d data and an average detonation velocity over the third and fourth charge diameters. The program is described fully in Section 3.1.1.

A new method of estimating the mean critical geometry, presently being evaluated, may prove to be successful in reducing the number of tests required to provide a statistical estimate. The method relies on the assumption that the attenuation rate of a fading detonation wave, at a given point or over a given region in the subcritical sample, is a simple function of the sample size. This approach, and the results of its application, are discussed in Section 3.1.2.

3.1.1 Computer Analysis -- D vs x/d Data

In the work under this contract, the principal evidence used in determining whether or not a sample sustained steady-state detonation is the record of detonation velocity vs reduced distance. In Section 3.4.4.2, an exception to this criterion is discussed that applies to materials such as unadulterated AP-PBAN propellant, for which the critical detonation velocity is near the hydrodynamic sound velocity in the material. In the adulterated-propellant formulations that comprise the samples used in the present program, the critical detonation velocities are sufficiently above the hydrodynamic sound velocity to justify application of the sustained-velocity criterion: A sample is considered to have detonated if, after approximately two diameters of travel, the detonation wave proceeds at a constant velocity over the remaining sample length; a sample is considered to have failed to detonate if the velocity of the detonation wave decreases in a nearly continuous manner along the full length of the sample. *

A statistical test for steady-state detonation over the lower several diameters has been programed as part of a computer program that reduces distance-time data to velocity-distance data and prints the results in tabular and graphical form. The statistical criteria for determining the occurrence of a sustained detonation are developed in the following text and a sample of their results is presented.

*In each critical-geometry test designed for this program, the sample length is at least four times the diameter or minimum cross-sectional dimension. Therefore, the sustained velocity must occur over approximately two diameters.

It is assumed that if steady-state detonation is to occur, the detonation velocity will approach a constant value at some determinable distance (x) away from the initiated end. The value of x is variable from sample to sample and test to test because it depends upon the overboostering level of the initiating stimulus and upon the charge diameter.

In this computer program, the initial value of x/d (the reduced distance in diameters) from which the computations progress, is part of the input data, in recognition of the need for flexibility. A linear least-squares fit to the velocity (D) vs x/d data first is calculated using those data obtained at all probe positions beyond the arbitrary start points except the last. (The numerical-differentiation method employed to determine velocity is not as accurate when applied to interior points. Thus, exaggerated and suspect values of velocity are commonly calculated at the end points.) The final exclusion of the end point is determined by comparing it with the least-squares predicted value, using the t-statistic

$$t = \frac{\hat{D} - D_{obs}}{s_{\hat{D}}} \qquad (1)$$

where $\hat{D}$ is the estimated velocity, D_{obs} is the observed velocity calculated through the numerical-differentiation process, and $s_{\hat{D}}$ is the standard deviation of the estimate. If the calculated value of t exceeds the theoretical value at the 0.05 significance level, the end point is excluded. Otherwise the point is included and the least-squares solution recomputed to fit all the data points.

The test of whether the event is a steady-state detonation is accomplished by applying another t-statistic to the hypothesis that the slope of the least-squares best-fit linear solution is not significantly different from zero. The statistic is

$$t = \frac{b}{s_b} \qquad (2)$$

where b is the estimated slope calculated by the least-squares fit and s_b is the standard deviation of that estimate, given by

$$s_b^2 = \frac{\Sigma (D - \hat{D})^2}{(n - 2) \Sigma (X - \bar{X})^2} \qquad (3)$$

where **X** = x/d and n equals the number of data points involved in the calculation. Since b is the slope of the line, this statistic has n - 2 degrees of freedom. If the calculated value of t exceeds the theoretical value at the 0.05 significance level, it is inferred that no steady-state detonation occurred.

The computer prints out on the tabular page the results of the statistical analysis of the velocity data. Included in this printout are: (1) the x/d starting point, (2) the number of points used in the calculation, (3) whether or not the end point was included, (4) slope of the least-squares fit solution, (5) standard deviation of the slope, (6) whether or not the slope is essentially zero, (7) average velocity, and (8) the standard deviation of the velocity data. An example of this printout is shown in Table 1.

3.1.2 Estimation of the Mean-Critical Geometry by Fading-Velocity Data

An investigation has been in progress to determine whether or not the fading detonation-velocity data generated in NO-GO tests could be used to estimate the critical geometry of a specified shape. It is assumed that attenuation in a sample very near the critical geometry, but subcritical, would proceed at a rather slow rate because of the almost sufficient size of the sample. A smaller size sample should cause the attenuation rate to be larger than in the above case because of greater curvature of the decaying reaction front and increased loss of energy by rarefaction waves. It is assumed further that over a certain (unspecified) range of subcritical sizes, the rate of attenuation may vary linearly with sample size. As a first approximation, the rate of attenuation has been derived as an average rate over a specific portion of the lower part of the charge.

The procedure consists of the following steps:

a. Compute the average detonation-velocity attenuation rate over the last several charge lengths of the NO-GO samples. This is calculated as being the slope of a least-squares line best fitting the velocity vs reduced distance data. (Technically, the average attenuation rate is the negative of this slope.)

Table 1. Detonation-Velocity Data, with Statistical Analysis for Sustainment Test 3.2.2.47.

TEST 3.2.2.47
TEST DATE 2 MAY 66
WITNESS PLATE GO

BATCH 2, 7.1 PERCENT RDX
SAMPLE 26
DIMENSIONS 6.48 IN DIA X 35.0 IN

*PROBE DATA, I3M ONLY

TIME SCALE FACTOR 1.00000 (USEC/UNIT) NR DATA PTS = 16
DIST SCALE FACTOR 1.00000 (INCH/UNIT) DIMEN = 6.48000 (INCHES)

TIME, T (USEC)	DISTANCE, S (INCHES)	REDUCED DIST, S/D (UNITLESS)	VELOCITY, V (MM/USEC)
2.15000	0.50000	0.07716	4.67495
13.29990	2.75000	0.42438	5.01000
24.44990	5.00000	0.77160	4.97344
35.59000	7.25000	1.11883	4.71763
48.53000	9.50000	1.46605	4.49633
61.76000	11.75000	1.81327	4.21077
75.26000	14.00000	2.16049	4.01855
89.15000	16.25000	2.50772	4.28966
102.85000	18.50000	2.85494	4.21719
115.80000	20.75000	3.20216	4.14705
129.92000	23.00000	3.54938	4.14030
143.78000	25.25000	3.89660	4.18314
157.68990	27.50000	4.24383	4.12088
171.60000	29.75000	4.59105	4.09971
185.31000	32.00000	4.93827	4.00431
199.80000	34.25000	5.28549	3.81149

STATISTICAL ANALYSIS OF VELOCITY DATA

BASED UPON LEAST SQUARES FIT STARTING AT L/D = 2.1605

NUMBER OF POINTS	END POINT INCLUDED	SLOPE OF LINE	ST. D. OF SLOPE	IS SLOPE EQ. ZERO	AVERAGE VELOCITY	ST. D. OF VELOCITY
9	NO	-0.03520	0.03237	YES	4.1422	0.069

b. Plot the slope vs sample size for all subcritical samples. Fit a least-squares line to these data.

c. Estimate the critical geometry for the shape by equating it with the dimension along the zero-slope ordinate intersected by the least-squares line.

This procedure has been applied to subcritical data from AAB-3225 propellant samples cast in Batch 4EH-84. The number of data points available in this case was eight. The graph of slope vs size is shown in Figure 1. From these data the estimated value of the critical diameter is 6.50 in.

Experimental evidence given by witness-plate appearance after the tests indicates that all samples of diameter equal to or greater than 6.48 in. were GO's; all samples of diameter equal to or less than 6.24 in. were NO-GO's. There was no overlapping or mixed-result regions. However, the computer program, which uses the statistical test for zero slope of the velocity-distance data to determine the GO's and NO-GO's, considered the 6.23 in. and the 6.24-in. diameter tests to be GO's, opposing the conclusions based on witness plate evidence. The reason for this contradiction rests in part with the oscillatory nature of the lower portion of each of these particular velocity-distance plots, resulting in a large computed standard deviation of the slopes that could not allow the statistical test to reject the hypothesis that the slope was zero. Nevertheless, it may still be true that the critical-diameter estimated from the reduced fading-detonation data is somewhat high.

A larger sample population became available when the critical-geometry tests of cylindrical and square-column shapes were completed. These tests involved nearly 50 samples of each shape. Twenty-nine samples of each shape were subcritical. The material was AAB-3189 adulterated propellant cast in Batch 4EH-86.

For each of the two shapes, the GO-NO GO results were overlapping. Hence, unique maximum-likelihood estimates of the mean-critical dimension could be calculated. Comparison of these estimates with those provided by the fading-velocity method constitutes the basis for judging the accuracy of the procedure.

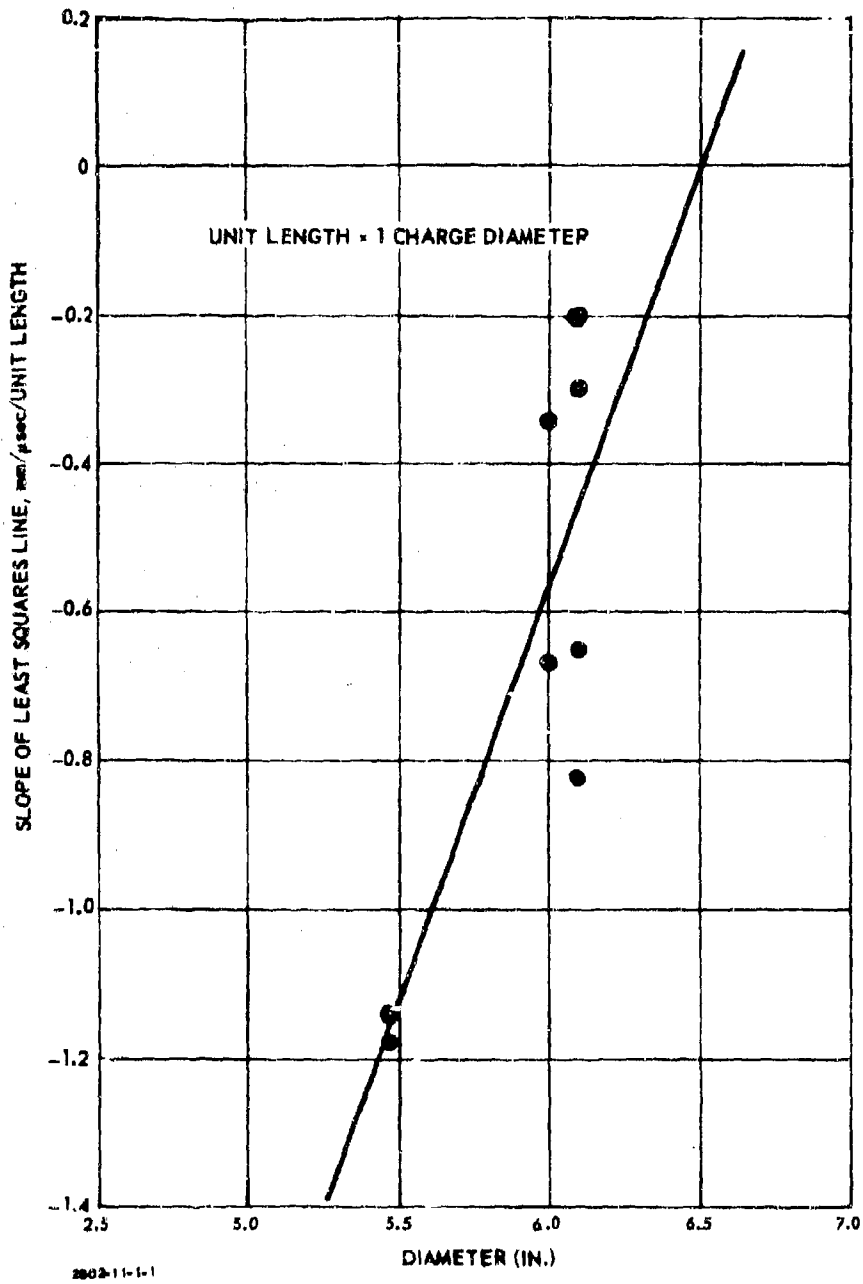

Figure 1. Critical Diameter Estimation for 7.1% Samples Batch 4EH-84.

The computed slope vs diameter data for the 29 subcritical cylinders, are presented in Figure 2. The least-squares best-fit line to these data, shown in the figure has this equation:

$$\delta = -6.907 + 2.403\ d \qquad (4)$$

where

δ = slope of velocity vs reduced distance

and

d = charge diameter

At $\delta = 0$, the estimated value of the critical diameter d_c is 2.87 in. The maximum likelihood estimate of d_c is 2.71 in. with an estimated standard deviation of 0.04 in. The former estimate clearly is four standard deviations greater than the latter. Statistically, the fading-velocity estimate fails in this case. It should nevertheless be noted that the difference in estimates of the mean is within 6% of the maximum likelihood estimate.

Figure 3 plots slope vs side dimension for the subcritical square-column samples. The least-squares best-fit line shown has the equation

$$\delta = -6.625 + 2.559\ s \qquad (5)$$

where s is the length of one side of the square cross section. At $\delta = 0$, the critical side of a square cross-section column is estimated to be 2.59 in. The maximum likelihood estimate of the critical dimension is 2.49 in., with a standard deviation of 0.04 in. Again, the former estimate is larger than the latter, in this case by 2.5 standard deviations (4%).

Statistically, the results of these trials show the present procedure to be unsatisfactory. However, the results are not discouraging, because several simplifications were made in the formulation of this procedure and revision of the procedure in accordance with theoretical considerations may yet facilitate its development into an accurate estimating tool.

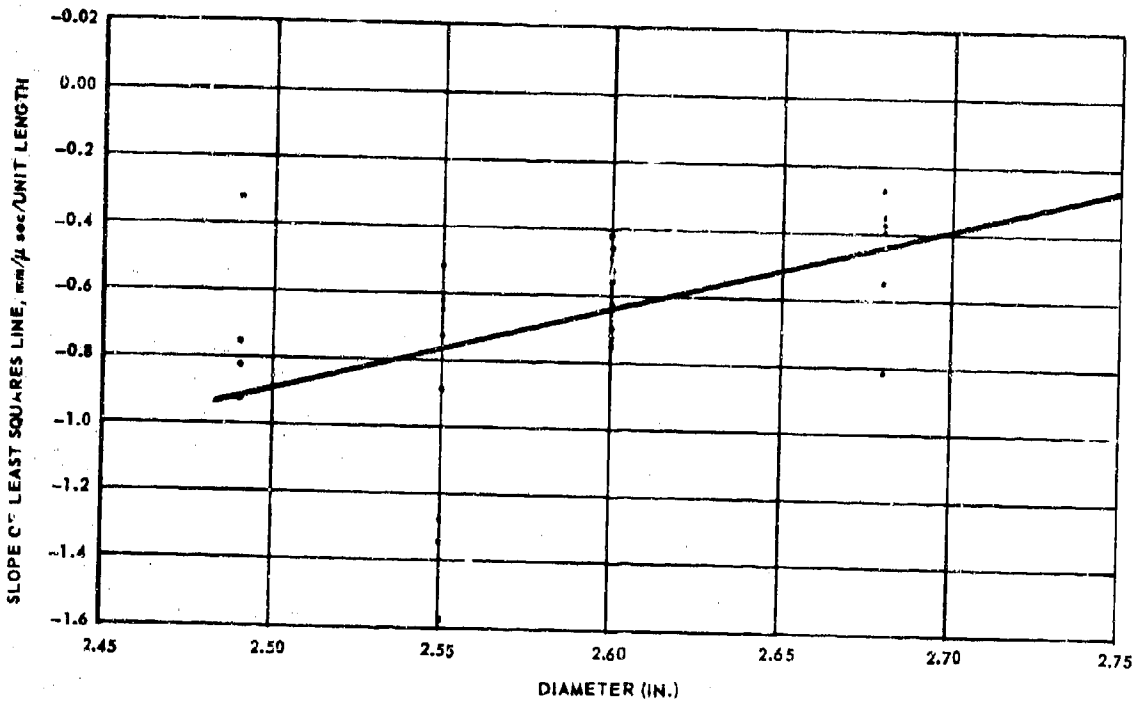

Figure 2. Critical Diameter Estimation from Fading Data for 9.2% RDX Samples, Batch 4EH-86.

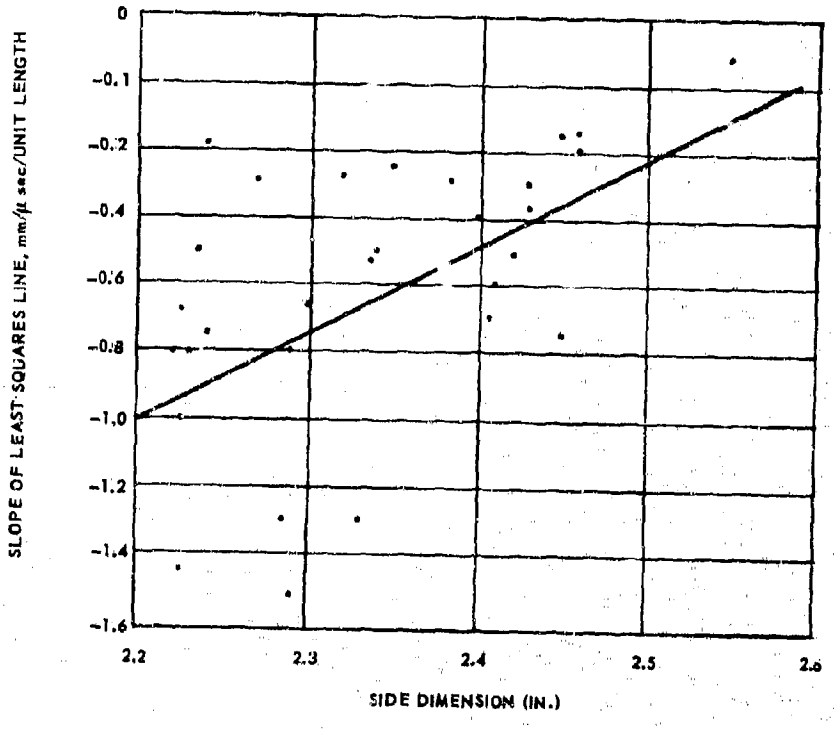

Figure 3. Critical Dimension Estimation from Fading Data for 9.2% RDX Samples, Batch 4EH-86.

One outstanding factor is immediately obvious: when mixed results occur, there may be NO-GO results at sizes larger than the maximum-likelihood estimated critical geometry. Such was the case in both of the test cases just discussed. The presence of nonzero data points at the supercritical sizes would be expected to cause the least-squares line to be biased in that direction. It appears that results obtained in the mixed-result region may be discarded legitimately when assembling data for analysis by the fading-detonation method.

3.2 THEORY OF CRITICAL GEOMETRY (PHASE I)

3.2.1 Variance and Mean-Critical Geometry

3.2.1.1 Test Objective

The object of this subtask is to evaluate the variance in critical-geometry test data obtained from circular-cylindrical and square-column shapes, cast from AAB-3189 (9.2 weight percent RDX) adulterated propellant. Knowledge of the magnitude of the variance, and the effect of sample shape on this quantity, are essential for the proper design of the critical-geometry tests that are to be performed in Subtasks 3.3.2 and 3.3.3. A large variance would require that sample sizes be selected that lay within the expected region of mixed results and that a particular distribution of these sizes be selected to permit an accurate estimation of the mean-critical geometry to be made. On the other hand, should the material exhibit a relatively small variance, of the order of the smallest increment in charge size that the particular series reasonably will allow, the number and distribution of the sample sizes that should be tested would be quite different from that required under the previous set of conditions.

Batch-to-batch variation also is studied in this subtask by statistically comparing the mean-critical diameters and the variances of all the batches cast. It is vital to be assured of minimal batch-to-batch variation before initiating an extensive critical-geometry test series.

3.2.1.2 Test Setup and Instrumentation

The critical-geometry test setup uses a high-explosive (Composition B) booster, the propellant acceptor, a mild steel witness plate, and an ionization-probe/rasteroscillograph instrumentation system. The booster is a solid right circular cone, of height equal to three base diameters. The acceptors are at least four diameters, or four square-side lengths high. In this particular subtask, the witness plate used is hot-rolled mild steel, 6-in. by 6-in. by 3/8-in. thick, supported at least 1 in. above the ground.

The ionization probes are inserted at points along the side of the test article to a uniform depth. Assurance of equal spacing and correct angular placement is by means of a machined guide bar that directs the tool that is used to form the holes in the sample into which the probes are put.

3.2.1.3 Test Results

Two acceptable batches of AAB-3189 propellant, that included samples tested under this subtask, have been cast since the program began. The nominal dimensions and numbers of samples at each dimension are shown in Table 2.

The results from the Batch 4EH-85 tests have been reported previously (Reference 1). A summary of the results obtained from an additional 48 critical-diameter tests (Batch 4EH-86) is given in Table 3. The samples are listed in order of increasing diameter, and, for those of the same diameter, in order of decreasing density. The Batch 4EH-86 GO-NO GO results are shown graphically in Figure 4.

Table 4 presents the results of 54 critical-geometry tests performed on the square column shapes cast in Batch 4EH-86. A graphical display of the GO-NO GO population is shown in Figure 5.

3.2.1.4 Data Analysis

Maximum likelihood estimates of the mean critical diameter and the standard deviation of the Batch 4EH-86 material are 2.71 in. and 0.04 in., respectively. Since there was one reversal in the square-column

Table 2. Sample-Size Distribution for the Variance and Mean-Critical-Geometry Subtask.

Shape	Nominal Size* (in.)	Number of Samples 4EH-85	Number of Samples 4EH-86
Circular Cylinder	2.50	-	5
	2.56	-	10
	2.62	20	10
	2.68	5	10
	2.74	5	10
	2.80	20	5
Square Column	2.20	-	6
	2.26	-	6
	2.32	-	6
	2.38	-	6
	2.44	-	6
	2.50	-	6
	2.56	-	6
	2.62	-	6
	2.68	-	6

*Diameter for circular-cylinder shape; length of side of square cross-section for square-column shape.

Table 3. Test Results, Subtask 3.2.1
Solid Cylindrical Samples.

Mear.	Standard Deviation (in.)	Density (gm/cc)	Result of Test	Average Detonation Velocity (mm/μsec)	Std Dev. of Velocity (mm/μsec)	Test No. 3.2.1
2.49	0.002	1.731	No-Go	-	-	76
2.49	0.001	1.728	No-Go	-	-	74
2.49	0.002	1.726	No-Go	-	-	77
2.49	0.002	1.722	No-Go	-	-	75
2.55	0.002	1.726	No-Go	-	-	79
2.55	0.003	1.725	No-Go	-	-	86
2.55	0.001	1.724	No-Go	-	-	81
2.55	0.002	1.723	No-Go	-	-	84
2.55	0.002	1.722	No-Go	-	-	85
2.55	0.001	1.722	No-Go	-	-	80
2.55	0.002	1.722	No-Go	-	-	78
2.55	0.002	1.721	No-Go	-	-	83
2.55	0.001	1.721	No-Go	-	-	82
2.55	0.002	1.721	No-Go	-	-	87
2.61	0.002	1.727	No-Go	-	-	96
2.61	0.001	1.725	No-Go	-	-	95
2.61	0.003	1.725	No-Go	-	-	93
2.61	0.001	1.725	No-Go	-	-	88
2.61	0.002	1.724	No-Go	-	-	97
2.61	0.002	1.724	No-Go	-	-	94
2.61	0.003	1.724	No-Go	-	-	91
2.61	0.002	1.724	No-Go	-	-	92
2.61	0.003	1.723	No-Go	-	-	89
2.61	0.003	1.721	No-Go	-	-	90
2.67	0.003	1.728	No-Go	-	-	99
2.67	0.002	1.727	No-Go	-	-	100
2.67	0.002	1.727	No-Go	-	-	104
2.67	0.002	1.726	No-Go	-	-	105
2.67	0.002	1.725	No-Go	-	-	101
2.67	0.002	1.722	No-Go	-	-	106
2.68	0.001	1.728	Go	4.12	0.23	103
2.68	0.001	1.727	Go	4.19	0.11	102
2.68	0.002	1.718	No-Go	-	-	98
2.74	0.004	1.732	No-Go	-	-	115
2.74	0.001	1.729	Go	4.21	0.10	111
2.74	0.001	1.729	Go	4.25	0.10	114
2.74	0.001	1.729	Go	4.25	0.10	113
2.74	0.003	1.728	No-Go	-	-	112
2.74	0.001	1.727	Go	4.25	0.03	109
2.74	0.001	1.727	No-Go	-	-	113
2.74	0.001	1.727	Go	4.29	0.06	108
2.74	0.001	1.726	Go	4.26	0.09	110
2.74	0.001	1.724	Go	(no record)	-	107
2.79	0.002	1.731	Go	4.21	0.11	120
2.79	0.004	1.725	Go	4.29	0.13	119
2.80	0.002	1.730	Go	4.27	0.06	118
2.80	0.003	1.729	Go	4.27	0.19	121
2.80	0.003	1.728	Go	4.16	0.10	117

Average Density 1.726 gm/cc
Standard Deviation 0.0031 gm/cc

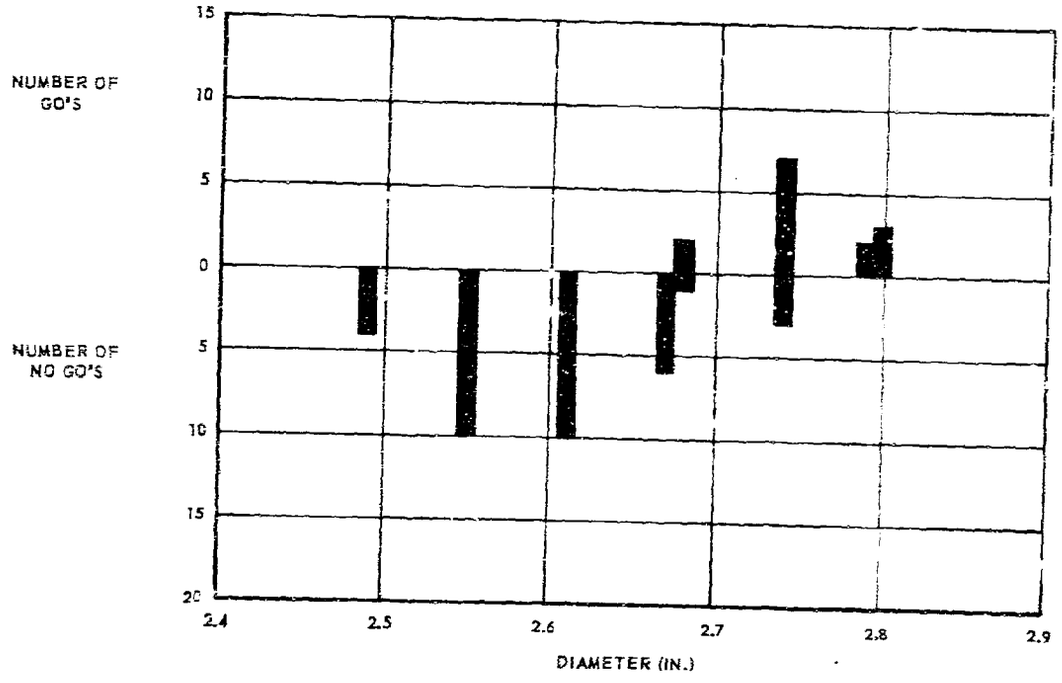

Figure 4. Critical Diameter Results Subtask 3.2.1
Batch 4EH-85.

Table 4. Test Results, Subtask 3.2.1
Solid Square Columns.

Side Dimension Mean (in.)	Side Dimension Std Dev (in.)	Density (gm/cc)	Result of Test	Average Detonation Velocity (mm/μsec)	Std Dev of Velocity (mm/μsec)	Test No. 3.2.1
2.22	0.012	1.726	No-Go	-	-	152
2.22	0.024	1.723		-	-	154
2.22	0.010	1.723		-	-	124
2.23	0.006	1.724		-	-	153
2.23	0.006	1.723		-	-	122
2.24	0.006	1.724		-	-	123
2.27	0.009	1.722		-	-	157
2.28	0.011	1.723		-	-	156
2.29	0.029	1.723		-	-	126
2.29	0.009	1.723		-	-	127
2.30	0.019	1.725		-	-	155
2.31	0.008	1.727		-	-	132
2.31	0.017	1.724		-	-	125
2.32	0.014	1.721		-	-	129
2.33	0.010	1.723		-	-	133
2.34	0.015	1.726		-	-	128
2.34	0.017	1.721		-	-	134
2.35	0.014	1.724		-	-	158
2.38	0.050	1.727		-	-	159
2.40	0.028	1.729		-	-	135
2.41	0.031	1.730		-	-	136
2.41	0.030	1.727		-	-	137
2.42	0.011	1.723		-	-	138
2.43	0.012	1.725		-	-	142
2.43	0.037	1.724		-	-	139
2.45	0.010	1.730		-	-	140
2.45	0.010	1.727		-	-	160
2.46	0.016	1.729		-	-	130
2.46	0.004	1.729	No-Go	-	-	141
2.50	0.015	1.728	Go	4.12	0.211	131
2.50	0.012	1.726	Go	4.23	0.075	146
2.50	0.018	1.723	Go	4.27	0.078	161
2.51	0.007	1.723	Go	4.16	0.281	145
2.53	0.015	1.728	Go	4.30	0.051	144

Table 4. (Continued)

Mean	Std Deviation (in.)	Density (gm/cc)	Result of Test	Average Detonation Velocity (mm/μsec)	Std Dev of Velocity (mm/μsec)	Test No. 3.2.1
2.54	0.010	1.727	Go	4.26	0.053	143
2.54	0.017	1.726	Go	4.31	0.124	162
2.55	0.014	1.723	No-Go	-	-	147
2.57	0.015	1.726	Go	4.28	0.111	164
2.58	0.024	1.728	Go	4.23	0.108	149
2.58	0.024	1.724	Go	4.28	0.078	163
2.60	0.010	1.726	Go	4.27	0.125	165
2.62	0.010	1.726	Go	4.28	0.053	148
2.62	0.013	-	Go	4.29	0.64	150
2.63	0.027	1.728	Go	4.35	0.046	169
2.63	0.025	1.725	Go	4.29	0.070	168
2.65	0.011	1.729	Go	4.35	0.064	167
2.68	0.021	1.727	Go	4.26	0.070	151
2.68	0.019	1.726	Go	4.34	0.069	166
2.68	0.022	1.725	Go	4.31	0.060	172
2.68	0.010	1.725	Go	4.30	0.091	175
2.68	0.016	1.723	Go	4.27	0.075	174
2.70	0.011	1.729	Go	4.29	0.087	173
2.70	0.008	1.726	Go	4.34	0.059	170
2.72	0.023	1.727	Go	4.32	0 054	171

Average Density 1.725 gm/cc
Standard Deviation 0.0023 gm/cc

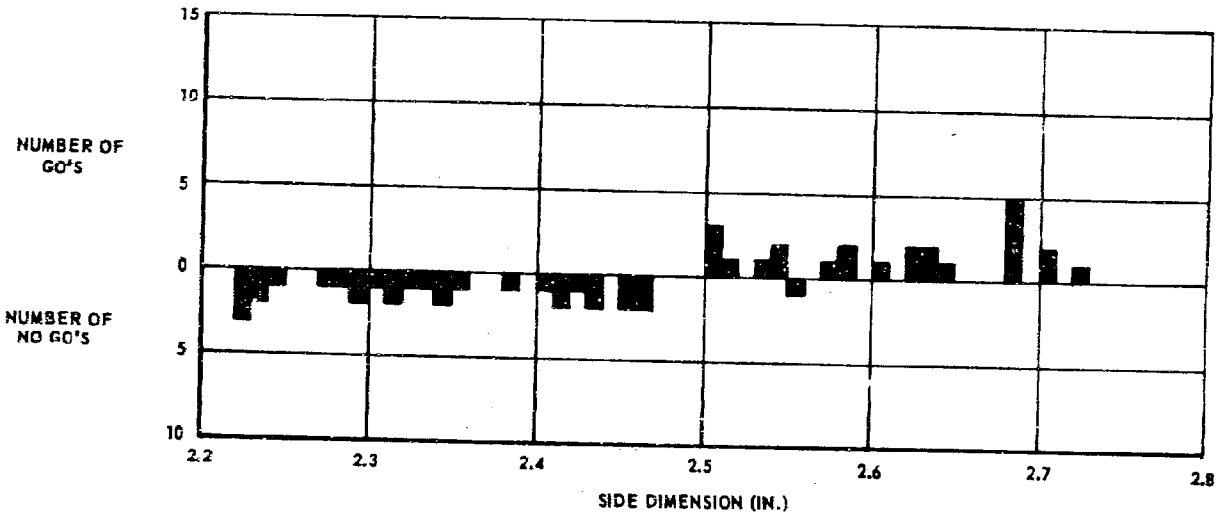

Figure 5. Critical-Geometry Results, Subtask 3.2.1 (square columns) Batch 4EH-86.

data (i. e., a NO-GO response occurring at a size greater than the smallest size at which a GO response was observed) maximum likelihood estimates of the mean critical geometry and the standard deviation can be calculated. These values are 2.49 in. and 0.04 in., respectively. Since the standard deviations from the two sets of data are identical, no statistical test of their similarity is necessary. It is concluded that variance, which is the square of the standard deviation, is independent of shape in this instance. Because the square is similar to the circle (i. e., solid, nonacute), extending this conclusion to all shapes would be unsound. Since a large number of equilateral triangular cross-section shapes will be tested in the critical-geometry subtask (see Section 3.3.2), it will be possible to evaluate the effect of shape on variance for an acute shape when those tests have concluded.

3.2.1.4.1 Evaluation of the Critical-Geometry Theory

The critical-geometry theory states that for a given material, there is one critical geometry for all shapes. The critical geometry is equal to 4A/P, where A is the cross-sectional area and P is the total perimeter of the critical size. For a solid circular cylinder, 4A/P = d, so that at the critical size, the critical geometry is the critical diameter. For a square cross-section, 4A/P = s, where s is the length of a side of the square. Therefore, the theory predicts that the critical geometry of a square shape is equal to the side length of the critical square. If the theory holds for squares and cylinders, s_c should be equal to d_c.

Combining all the critical-diameter data compiled on AAB-3189, including that generated under Contract AF 04(611)9945, the mean critical diameter is 2.66 in., with a standard deviation of 0.080 in.

Comparison of the predicted 2.66 in. with the experimental mean square critical geometry of 2.49 in. shows the theory predicts a critical geometry approximately 6% too large for the square. Using 2.71 in., the critical diameter of Batch 4EH-86, the comparison shows an overestimate by the theory of approximately 8%. These findings are completely consistent with those found for the same material under Contract AF04(611)9945, SOPHY I (Reference 2). From the SOPHY I data, however, the overestimation seems to be the same for all nonsolid-cylindrical shapes, which implies that there is one critical geometry for all such shapes and that its value is approximately 0.92 d_c.

3.2.4.2 Batch-to-Batch Variations

Since statistical tests of the SOPHY I data and that from Batch 4EH-85 (Reference 1) showed batch-to-batch differences, Batch 4EH-86 was cast to investigate the variation more fully. Comparative statistics from the three populations are shown in Table 5, and a graph of the combined GO-NO GO results is shown in Figure 6. It should be pointed out that the SOPHY I data, although it is treated as one population, actually includes the combined results from three batches of propellant. The total number of samples, however, is still much less than the number tested in either of the recent batches. Also, the SOPHY I material was mixed and cast on a different line area at Sacramento; the batch size was 800 lb, compared to the 2000-lb batch size in SOPHY II. Different mixing equipment and personnel were used in the previous effort. It might be expected that under these circumstances, with the large number of differences between the two casting operations, the data could reflect the introduction of such parameters.

Inspection of Table 5 reveals that the results from Batch 4EH-86 are almost identical to those from SOPHY I. In fact, the 95% confidence ellipses for the mean (μ) and the standard deviation (σ), calculated for this batch, is completely contained within the ellipse drawn from the SOPHY I data (Figure 7). This figure shows the ellipse drawn for Batch 4EH-85 as well, and the data indicate that a significant difference does exist between this batch and the two other sets of data.

Another statistical test, the likelihood ratio statistic, shows that the three sets do not come from populations with the same cumulative normal response function. This test states that $-2 \ln\lambda$ follows the chi-square distribution approximately, where

$$\ln\lambda = \ln L_0 - \ln L_1 - \ln L_2 - \ln L_3 \qquad (6)$$

L_0 is the maximized sample likelihood of the combined set of data and L_1, L_2, and L_3 are the maximized sample likelihoods for the individual sets. In this case, the chi-square distribution has three degrees of freedom. Substituting in Equation 6 the ln-likelihoods presented in Table 5,

$$\ln\lambda = -20.12 \qquad (7)$$

Table 5. Comparison of Critical-Diameter Estimates
9.2% PDX Adulterated Solid Cylindrical Samples

Estimate of Quantity	Symbol	SOPHY I AF04(611)9945	SOPHY II Batch 4EH-85	SOPHY II Batch 4EH-86	All Data Combined	4EH-85 Combined with 4EH-86
Mean (in.)	μ	2.71	2.59*	2.71	2.66	2.65
Standard Deviation in.	σ	0.06	0.04*	0.04	0.08	0.08
Covariance, sq in.	$\sigma_{\mu\mu}$	0.00053	-	0.00016	0.00014	0.00017
	$\sigma_{\mu\sigma}$	0.00001	-	0.000004	0.00002	0.00002
	$\sigma_{\sigma\sigma}$	0.00052	-	0.00014	0.00017	0.00019
ln Likelihood	ln L	-6.46	-8.65*	-11.00	-47.53	-39.11

*Not maximum - likelihood estimates; Reference 1.

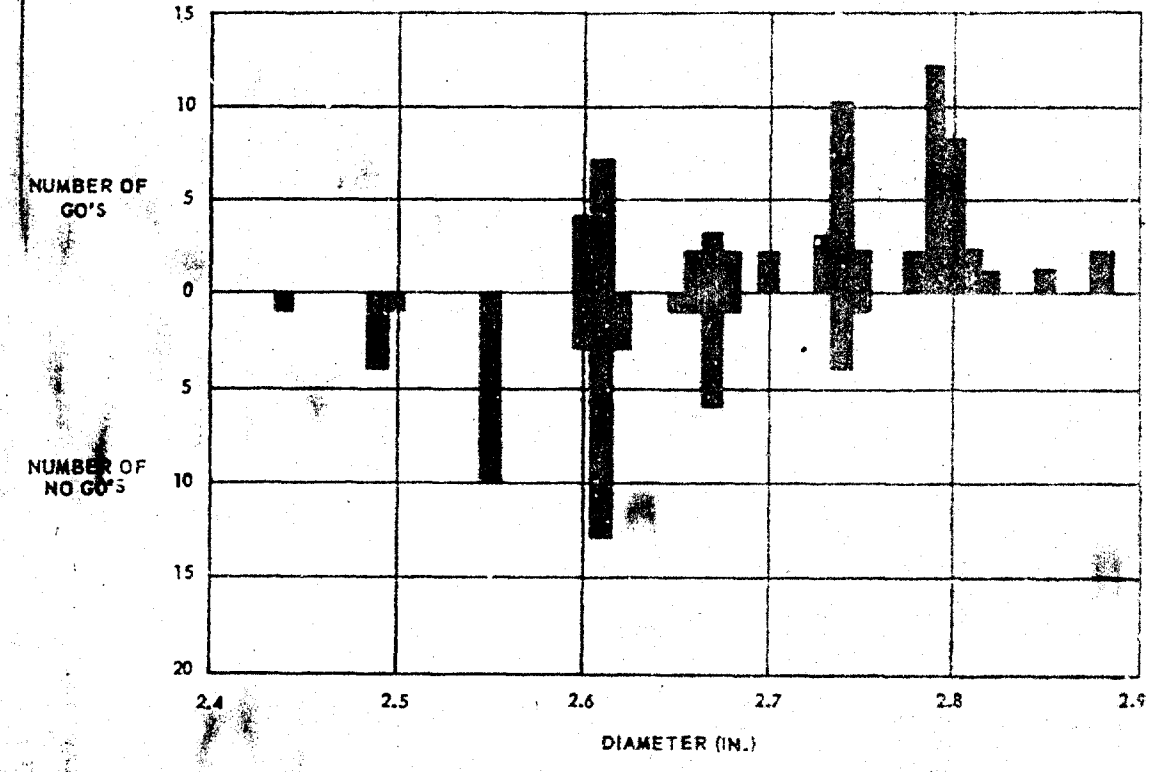

Figure 6. Combined Results SOPHY I and SOPHY II 9.2% RDX Adulterated Solid Cylindrical Samples.

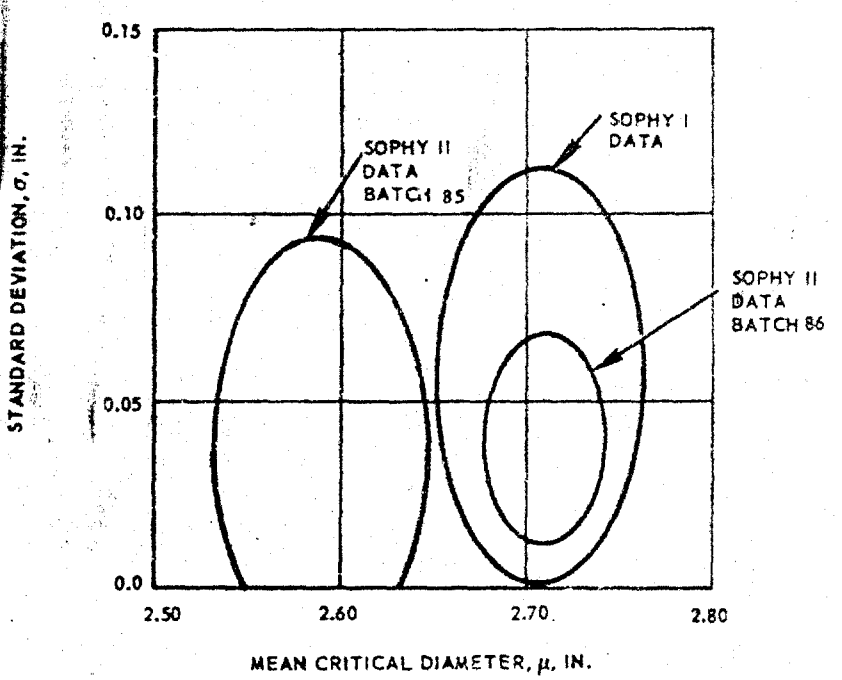

Figure 7. 95% Joint Confidence Ellipses for μ and σ.

Therefore, $\chi^2 = 40.24$. The probability of observing this value with three degrees of freedom is less than 0.0001. It must be inferred by this test that the samples do come from different populations.

The within-batch standard deviations for Batches 4EH-85 and -86 are identical (Table 5). The standard deviation from the SOPHY I data includes batch-to-batch variation as well as within-batch variation, since it is a pooled set of data from three batches. Similarly, when all the AAB-3189 data are pooled, giving a mean critical diameter of 2.66 in., the standard deviation (0.08 in.) contains both the within-batch and the batch-to-batch variations. Subtracting the within-batch variance (0.0016-in. squared) from the total variance (0.0064-in. squared), the batch-to-batch standard deviation is estimated to be 0.07 in.

In all these calculations, the standard deviation resulting from the measurement errors and dimensional nonuniformity is one order of magnitude less than those calculated from the GO-NO GO data. The effect of these human errors is therefore trivial.

3.2.2 Mean Critical Diameter and Variance

3.2.2.1 Test Objectives

The prime objectives are to obtain sufficient data to provide (1) an accurate estimate of the mean critical diameter and (2) a reasonably good estimate of the variance. The first objective must be achieved because this composition will be used later in Phase 2 tests to verify the critical-geometry theory. The critical-diameter value at this RDX weight percent will be useful in the further development of the theoretical model of detonation. The second objective is required for the verification-tests design. It will provide a preliminary basis for estimating the effect of sample size on the variance of critical-diameter data.

3.2.2.2 Test Setup and Instrumentation

The setup and instrumentation for these tests are identical to that in Subtask 3.2.1 except that the witness plate is a 12-in. by 12-in. by 3/8-in. thick plate. The larger plate is required because the samples have twice the diameter of the AAB-3189 samples. The material used under this subtask is AAB-3225, which is an AP-PBAN formulation adulterated with 7.1 weight % RDX.

3.2.2.3 Test Results

Three batches of AAB-3225 have been cast for this subtask. Results from the two previous batches, 4EH-44 and 4EH-84, have been reported in previous quarterly reports (References 3 and 1, respectively).

Batch 4EH-107 was cast to provide additional information on the apparently large batch-to-batch variation in the mean critical diameter of this material. The test design for this third batch was identical to that for Batch 4EH-84 (Reference 1).

The results of the tests are shown in Table 6. The need to cover a large range of diameters in this test design precluded the casting of more than two samples at any of these sizes because of their weight and the 2000-lb limit on batch size. The test results are composed of nine GO-NO GO data points. Testing at the larger sizes (greater than 5.75 in.) serves no purpose once the critical region is established to be at 5.25 in.

3.2.2.4 Data Analysis

3.2.2.4.1 Calculation of μ and σ

Mixed results occurred only at the 5.25-in.-diameter. For results of this type, the maximum likelihood estimate of the mean is given by the test level at which the mixed results occur, 5.25 in.; the maximum likelihood estimate of the standard deviation must be zero. The latter estimate is difficult to accept. One estimate that appears to be more realistic is that obtained by combining estimates derived from two other estimation techniques, i.e., the minimum overlapping subset method and the two subset method (Reference 4). Applying these techniques to the data yields an estimate of the standard deviation of 0.07 in.

3.2.2.4.2 Comparison with Previous Data

Summary statistics from all three batches of 7.1% RDX adulterated solid cylindrical samples are shown in Table 7. It is obvious that the results obtained from Batches 4EH-44 and -107 agree quite closely and that they disagree strongly with the results obtained from Batch 4EH-84.

Table 6. Test Results, Subtask 3.2.2 (Batch 4EH-107).

Mean Diameter (in.)	Result of Test	Average Detonation Velocity (mm/μsec)	Std Dev of Velocity (mm/μsec)	Test No.
5.00	No-Go	-	-	3.2.2.59
5.01	No-Go	-	-	3.2.2.57
5.24	No-Go	-	-	3.2.2.58
5.25	Go	4.08	0.095	3.2.2.56
5.49	Go	4.17	0.072	3.2.2.55
5.49	Go	4.11	0.135	3.2.2.60
5.74	Go	4.23	0.081	3.2.2.61
5.75	Go	4.17	0.163	3.2.2.54
5.99	Go	4.26	0.124	3.2.2.53

Table 7. Comparison of Critical-Diameter Estimates 7.1% RDX Adulterated Solid-Cylindrical Samples.

Estimated Quantity	Symbol	Batch 4EH-44	Batch 4EH-84	Batch 4EH-107	Combined Data Batches 4EH-44 and -107
Mean (in.)	μ	5.21	6.36*	5.25	5.24
Standard Deviation	σ	0.06	-	0.07	0.03
Covariance	$\sigma_{\mu\mu}$	0.00247	-	-	0.00031
	$\sigma_{\mu\sigma}$	-0.00196	-	-	0.00026
	$\sigma_{\sigma\sigma}$	0.00197	-	-	0.00035
ln Likelihood	ln L	-8.15	-	-1.39	-10.13

*Not maximum-likelihood estimate; see Reference 1.

A statistical test of the hypothesis that the data from Batches 4EH-44 and -107 come from populations with identical cumulative normal response functions can be made using the likelihood-ratio criterion described in Paragraph 3.2.1.4. For these data, the ln-likelihood ratio is calculated as

$$\ln\lambda = -10.13 + 8.15 + 1.39 \quad (8a)$$

$$= -0.59 \quad (8b)$$

Therefore,

$$\chi^2 = 1.18 \quad (9)$$

The probability of observing a chi-square value of this size with two degrees of freedom is approximately 0.55. Hence, it is concluded that both sample batches come from populations with the same cumulative normal response function.

An exact statistical comparison of all three batches is somewhat difficult since it was impossible to calculate a likelihood for the Batch 4EH-84 samples. However, the fact that the mean of this batch differs significantly from the means of the other two batches is obvious; the batch means differ by more than 1 in. with a within-batch standard deviation of 0.07 in. It is statistically hard to believe that this large of a variation in batch means could be attributable to normal batch-to-batch variation. In fact, applying the Dixon-Mood criteria for extreme means to this data (Reference 5) it can be shown at the 0.05 significance level that the Batch 4EH-84 mean is a statistical outlier with respect to the other two means.

Since the large difference in mean critical diameter exists between Batch 4EH-84 and the other two batches, some explanation is required. To this date, all efforts at identifying a chemical or physical difference have been unsuccessful. The compositions of the three batches, as judged from the preparation data, are identical. Furthermore, Batch 4EH-44 was bayonet cast, while the other two were vacuum cast. X-ray reports show that only Batch 4EH-44 samples contained large amounts of pores visible by this technique, yet microscopic examination of samples from this batch could not detect porosity in the 12 to 100μ-diameter pore-size region. Density measurements on sections from samples remaining from all three batches are being performed to discover whether there is a correlative difference in sample density between the batches.

3.2.3 Detonation Velocity as a Function of Size

3.2.3.1 Test Objective

In developing the Aerojet detonation model (Reference 2), a modified Jones detonation model was used. The purpose of this subtask is to determine the validity of the Jones-type model to composite adulterated propellant and to determine further the perturbations to the model that may be required when investigating a noncylindrically shaped sample. In this case, the square cross-section column was chosen to test the model's applicability.

3.2.3.2 Test Setup and Instrumentation

The setup is similar to that used in Subtasks 3.2.1 and 3.2.2. The three exceptions which hold in the tests under discussion here are (1) no witness plate is employed since all samples are supercritical, (2) the probes are distributed to instrument the lower half of the sample since the object of the test is to determine the average detonation velocity, and (3) one or two conductance probes are used to obtain data that may provide a means of measuring the reaction-zone thickness. Description of the conductance probe method has been given in a previous report (Reference 3). The propellant formulation is AAB-3189.

3.2.3.3 Test Results

The results of the detonation-velocity measurements in the cylindrical and square-column shapes are shown in Table 8. The conductance-probe measurements are shown in Table 9. The average detonation velocity and conductance-zone length for each size is presented in Table 10.

Table 8. Average Detonation Velocities for Supercritical 9.2% RDX Calibrated Samples.

A. Solid Circular Cylinders

Size (in.)	Average Velocity (mm/μsec)	Std. Dev. of Velocity (mm/μsec)	Test No.
12 (dia)	4.74	0.180	3.2.3.1
	4.77	0.100	3.2.3.2
	4.77	0.083	3.2.3.3
8	4.70	0.065	3.2.3.4
	4.71	0.035	3.2.3.5
	4.71	0.081	3.2.3.6
	4.70	0.110	3.2.3.7
	4.67	0.160	3.2.3.8
	4.72	0.029	3.2.3.10
	4.69	0.012	3.2.3.11
6	4.62	0.096	3.2.3.23
	4.68	0.140	3.2.3.28
	4.52	0.085	3.2.3.37
4 (dia)	4.46	0.086	3.2.3.25
	4.48	0.051	3.2.3.31
	4.54	0.100	3.2.3.35

B. Solid Square Columns

6.0 (side)	4.62	0.057	3.2.3.27
	4.64	0.049	3.2.3.22
	4.64	0.197	3.2.3.38
4.5	4.63	0.105	3.2.3.21
	4.55	0.077	3.2.3.26
	4.54	0.001	3.2.3.36
	4.56	-	3.2.3.30
3.5	4.53	0.091	3.2.3.19
	4.45	0.046	3.2.3.24
	4.45	0.121	3.2.3.29
	4.44	0.035	3.2.3.34
3.0 (side)	4.39	0.029	3.2.3.15
	4.44	0.085	3.2.3.16
	4.47	0.244	3.2.3.17
	4.36	0.082	3.2.3.18

Table 9. Conductance-Probe Measurements, Subtask 3.2.3.

Test No. 3.2.3-	Size (in.)	Detonation Velocity (mm/μsec)	Pulse Width (μsec)	Conductance-Zone Thickness (in.)
		Cylinders		
1	12 (dia)	4.74	No data	No data
2	12	4.77	No data	No data
3	12	4.77	56	10.5
4	8	4.70	33	6.1
5	8	4.71	37	6.8
6	8	4.71	37	6.8
7	8	4.70	50	9.2
8	8	4.67	30	5.6
9	8	No data	34	No data
10	8	4.72	38	7.0
11	8	4.69	50	9.2
23	6	4.62	40	7.3
28	6	4.68	42	7.2
33	6	No data	40	No data
37	6	4.52	40	7.3
20	4	No data	40	7.1
25	4	4.46	34	6.0
31	4	4.48	32	5.6
35	4 (dia)	4.54	32	5.6
		Square Columns		
22	6 (side)	4.64	35	6.4
27	6	4.62	33	6.0
38	6	4.65	Not clear	No data
21	4.5	4.63	30	5.4
26	4.5	4.55	33	5.9
30	4.5	No data	30	No data
36	4.5	4.54	32	5.8
19	3.5	4.53	22	3.9
24	3.5	4.45	30	5.3
29	3.5	4.45	Not clear	No data
34	3.5	4.44	30	5.3
15	3	4.39	14	2.4
16	3	4.44	13	2.3
17	3	4.47	22	3.8
18	3 (side)	4.36	22	3.8

Table 10. Average Detonation Velocity and Conductance-Zone Length.

Size (in.)	Average Detonation Velocity (mm/μsec)	Average Conductance-Zone Length (in.)
12 (dia)	4.76	10.5*
8	4.70	7.0
6	4.61	7.2
4 (dia)	4.49	6.1
6 (side)	4.64	6.2
4.5	4.57	5.6
3.5	4.47	4.8
3 (side)	4.42	3.1

*This is the result of one test and should be so weighted.

3.2.3.4 Data Analysis

3.2.3.4.1 Correlation of Detonation Velocity and Size

The refined detonation model presented in Reference 2, Equation 18, states that

$$d = \frac{kD\left(\frac{d_{RDX}}{2}\right)\left[\left(\frac{G}{f+c}\right)^{1/3} - 1\right]}{B\left[1 - (D/D_i)^2\right]^{1/2}} \qquad (10)$$

where

d	=	charge diameter
D	=	detonation velocity
d_{RDX}	=	average RDX particle diameter
c	=	equivalent weight fraction RDX to account for other hot-spot initiation sites
f	=	weight fraction RDX
B	=	Arrhenius rate expression for the linear pyrolysis kinetics of ammonium perchlorate (AP)
D_i	=	ideal detonation velocity
k, G	=	constants

B can be expressed as a function of T_s, the surface temperature of the regressing AP particles,

$$B = 0.00021\ T_s \exp(-21,500/RT_s) \qquad (11)$$

and T_s can be expressed as follows:

$$T_s = 1824 + 18.4\ \rho_o\ D^2 - 0.137\ \rho_o^2\ D^4 \qquad (12)$$

where ρ_o is the AP bulk density in the charge.

Equation 10 can be reduced, therefore, to an expression for d as a function of one parameter, the detonation velocity D. A computer program is being written that will use the detonation-velocity data and calculate corresponding diameter data. Correlation of the calculated diameters (d_{calc}) and the experimentally measured diameters (d_{exp}) will be printed out, for visual interpretation, as a d_{calc} vs d_{exp} plot, with a straight line through the origin of slope equal to one for reference. Other plots that will be printed include (1) a D vs d_{calc} curve with the (D, d_{exp}) points plotted and (2) a g(f) vs d_{calc} curve with the ($g'f$), d_{exp}) points plotted. The g(f) function (Reference 2, Equation 26) is given by

$$g(f) = \frac{D}{B\left[1-(D/D_i)^2\right]^{1/2}} \qquad (13)$$

Correlation of the experimental data with that calculated will justify the use of the modified Jones detonation model in the SOPHY program. These calculations will be made for both shapes tested.

The velocity data presented in Table 8, when plotted against a reduced diameter (d/d_c) or reduced square-side dimension (s/σ_c), gives an interesting correlation between the two shapes (Figure 8). By normalizing the data in this manner, one curve can be generated, which fits both sets of data.

The theory of critical geometry states that for a given material there is a critical geometry that is the same for all shapes. The critical geometry is defined by

$$\sigma_c = \left(\frac{4A}{P}\right)_c$$

Where

σ_c is the critical geometry

A is the cross-sectional area

P is the total perimeter

and the subscript c refers to the critical size.

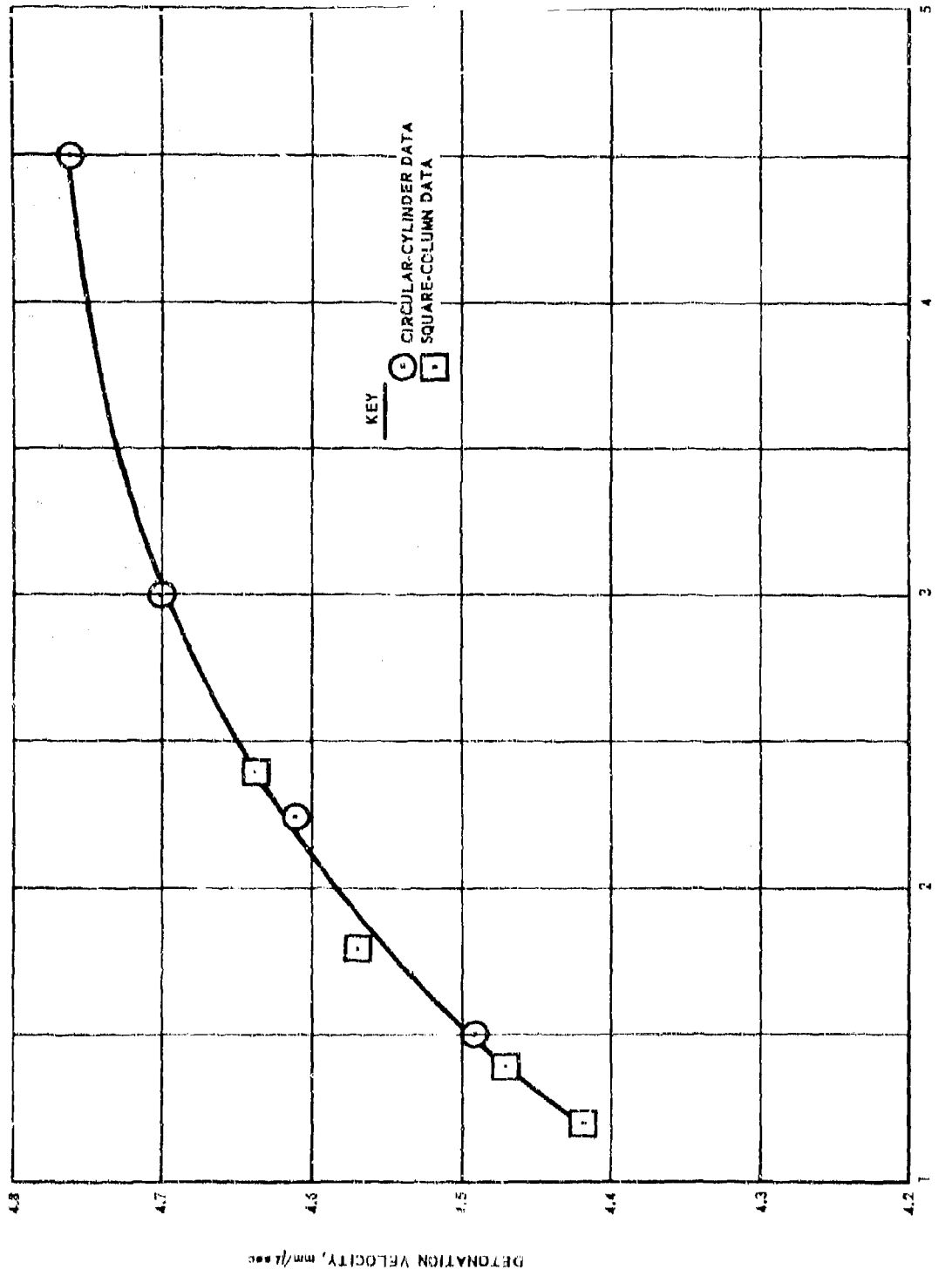

Figure 8. Average Detonation Velocity vs Reduced Size, Circles and Squares, AAB-3189, Subtask 3.3.2.

The theory also states that $\sigma_c = d_c$, the critical diameter. However, the implication from SOPHY I tests is that σ_c is nearly constant for a variety of noncircular-cylindrical shapes, but it is smaller than d_c by 6 to 8%. Therefore, the appropriate means of obtaining normalized-size data for a given shape would be to divide 4A/P by σ_c. For the special case, the solid circular cylinder, the normalized diameter should be obtained by dividing 4A/P by d_c. For the circle and the square, 4A/P equals d and s, respectively. Therefore, in Figure 8, the abscissa is d/d_c and s/σ_c.

3.2.3.4.1 Conductive-Zone Lengths

A study of the conductance probe and its use in determining reaction-zone thickness made obvious the need for more intensive theoretical analysis of the conditions most likely to exist in the high-conducting region found in detonating propellant.

The bulk of investigations into the use of conductance probes for reaction-zone measurement have been concerned with high explosives (Reference 6). In high explosives the reaction-zone thickness, which is the distance from the detonation front to the C-J surface, is very small compared to the distance from the detonation from to the axial intersection of the rarefaction regions. Since high explosives are generally either composed of one homogeneous compound or two highly reactive species, their reaction times are very short.

Little continuing reaction should be expected behind the C-J surface; subsequently, there should be a rapid decrease in the conductivity level behind this surface. Under these conditions conductivity probes should faithfully map the reaction zone.

In the case of composite propellants, however, reaction times are much longer and many side reactions occur. It is difficult to believe that the C-J surface, in a propellant detonation, would include before it the region in which all these reactions reached completion. Instead, the highly ionized region in which these reactions are progressing may quite logically extend behind the C-J surface. Conductance probe measurements made in composite propellant samples may be recording a region of greater thickness than the defined reaction zone. This possibility has occasioned the substitution of conductance-zone length for reaction-zone length in describing the experimental data generated by the conductance probes. Further study of the problem is in progress.

3.2.4 Jetting Phenomena Study

3.2.4.1 Test Objective

Critical-geometry tests on hollow-core cylinders, using end-on booster initiation techniques modified for this type of acceptor shape, revealed that a new phenomenon was occurring (Reference 2). In brief, sustained detonation was observed to degenerate into a fading detonation when samples were tested that had web thicknesses larger than the predicted critical thickness. Web thickness describes the distance from the inner surface to the outer surface of a hollow-core sample. The length of the charge over which the detonation was sustained increased when thicker webs were tested. Eventually a sample was tested that had enough material in its web to permit the sustained detonation to continue to the bottom end of the sample.

It was proposed that the reason for the unusual behavior of the hollow charges was the unavoidable formation of a jet within the core, formation was unavoidable because of the requirement that no confinement be applied to the samples being tested.

The object of this subtask is to study detonation in hollow core samples with appropriate instrumentation to provide data from which the jetting phenomenon and its effect on the detonation behavior can be better understood. Specifically, the effect of core diameter on the propellant reaction in samples having identical web thicknesses will be studied.

Also to be studied is the question of whether any small-diameter-core hollow cylinder can be considered supercritical in the classical sense, i.e., is it possible for there to be a finite web thickness for such a sample which will sustain detonation over an infinite length when sufficiently initiated? The pertinence of this question results because in the critical-geometry tests scheduled for SOPHY II, inner diameters of the hollow-core cylinders will be 1.5 and 3 in. If such a size sample can be expected to form a jet that does cause the longitudinally-directed detonation wave to attenuate at some point, dependent on the web thickness, it is clear that there will be no real critical geometry because no supercritical region exists.

3.2.4.2 Setup and Instrumentation

The hollow-core sample will stand on a suitable size witness plate and be initiated at the top by a solid, conical, high-explosive booster, except for the exceptionally large ID samples, which will be initiated by a specially-designed annular-shape booster. To prevent jet formation by the booster, either a Plexiglas plate will be placed between the booster and the acceptor charge or a plug will be inserted or cast into the ID at the initiated end of the acceptor.

Ionization probes will be inserted into the propellant sample perpendicular to the axis of the charge. One column of probes will have their tips aligned to coincide with the axis, the second column will be inserted a distance equal to 2/3 of the web thickness, and the third column will be inserted to a distance equal to 1/3 of the web thickness. Each column will be monitored by a different rasteroscilloscope and a common time reference will be furnished by a pulse delivered simultaneously to each scope soon after the scopes are triggered to sweep. In this way data will be accumulated that will permit a mapping of the detonation wave and jet positions at various times. The effect of the jet on the shape and orientation of the detonation wave will then be revealed.

3.2.4.3 Current Status

The samples have been cast and will be tested in September. Table 11 shows the dimensions of the samples and the number of samples at each size that have been cast. The propellant formulation is AAB-3189. The critical-geometry theory, which does not account for interactions such as have been seen to exist in samples of this shape, predicts a critical web thickness of 1.25 in. ($1/2\ \sigma_c$).

3.3 THEORY OF CRITICAL GEOMETRY (PHASE 2)

3.3.1 Detonation Velocity as Function of Size

This subtask is designed to be an extension of the study in Subtask 3.2.3, to be initiated if the results from Subtask 3.2.3 indicate that sample geometry affects the relationship between size and the detonation velocity

Table 11. Sample Size and Distribution for the Jetting Phenomena Study, AAB-3189.

Test Group*	No. of Samples	ID (in.)	Nominal OD (in.)	Length (in.)
A	4	0.06	2.9	14
A	4	0.12	3.0	14
A	4	0.25	3.1	14
A	4	0.50	3.6	14
A	4	0.75	3.6	18
A	4	3	5.8	24
A	4	6	8.8	36
B	4	1.5	4.5	18
B	4	1.5	4.5	22
B	4	1.5	4.5	28
B	4	1.5	4.5	36

*Test Group A; Web thickness constant, ID varied.

Test Group B; Size constant, length varied

and reaction-zone thickness. In order to fill the propellant batch from which samples for the triangular critical-geometry and the jetting phenomenon subtasks were cast, several supercritical triangular samples were cast so that they would be available for use under this subtask. These samples will be tested in September.

All the molds for the remainder of the samples intended for this subtask have been fabricated, so that as soon as the results from Subtask 3.2.3 are analyzed, it will be possible to initiate plans to cast them if needed. The other shapes include circular-core and cross-shaped-core hollow cylinders, with two different perforation sizes for each shape. The propellant formulation is AAB-3189.

3.3.2 Critical Geometry

3.3.2.1 Test Description

The purpose of these tests is to evaluate the critical-geometry model, $\sigma_c = (4A/P)_c$, for several shapes. It is a more intensive study than that performed under Contract AF04(611)9945, to provide better estimates of the mean critical geometry for each shape. The solid samples will be of two cross-sectional shapes: the equilateral triangle and the rectangle. The hollow-core circular-cylindrical samples will be circular-core and cross-core shapes, with each shape tested in two different size perforations. The sample formulation is AAB-3189.

The standard critical-geometry test setup will be employed, using boosters of cross-section matching that of the solid shapes, i.e., triangular and rectangular cross-sections; for the hollow-core samples, the booster arrangement will be similar to that employed in Subtask 3.2.4. The criterion for detonation in the solid shapes will be the observance of a sustained detonation velocity over the lower half of the sample. The interpretation of the hollow-core sample data will depend on the results of the jetting phenomena study in Subtask 3.2.4.

3.3.2.2 Progress

All molds for this subtask have been fabricated and propellant casting operations have begun. Several 2000-lb batches are required to prepare these samples. Each batch will contain eight solid-cylindrical samples, in sizes near the mean critical diameter, to provide an estimate of the mean critical diameter of the batch. The numbers and dimensions of the samples being prepared for this series are given in Table 12.

Since the critical-geometry theory states that the critical side of an equilateral triangular column, b_c is given by

$$b_c = \sigma_c \sqrt{3} \tag{14}$$

selection of 0.10-in. increments in b will permit the calculation of σ_c to within 0.06 in. maximum.

In determining the critical geometry of a rectangular cross-section shape, the technical approach this year will differ from that adopted under Contract AF04(611)9945. In the previous program (Reference 2) the various samples all were cast having the same width and length but different thicknesses. The object was to determine the critical thickness for the width being tested. Using the critical-geometry theory under this set of test conditions, the predicted critical thickness t_c would be given by

$$t_c = \left(\frac{x+1}{2x}\right) \sigma_c \tag{15}$$

where x is the ratio of width to thickness ($x > 1$ for rectangle) and σ_c is the critical geometry of the material. From Equation 15 it is clear that t_c is always less than σ_c. When testing a series in which the variable is smaller than σ_c, the increments in which that variable (t) is taken must be similarly smaller than the increments in which σ_c was determined, to preserve the same accuracy in the two determinations and permit meaningful comparison between the t_c (experimental) and the t_c (predicted). Increments in critical-diameter tests this year are approximately 1/16 in. A difficult situation would exist if the rectangular cross-section samples were tested in the SOPHY I design, because increments below 1/16 in. in thickness require dimensional tolerances tighter than can be economically applied to the rectangular shapes.

Table 12. Critical-Geometry Sample Description, AAB-3189.

Equilateral Triangular Cross-Section

No. of Samples	Side of Triangle, b (in.)	Sample Length (in.)
5	4.05	20
5	4.15	20
5	4.25	20
5	4.35	20
5	4.45	20
5	4.55	20

Rectangular Cross Section

No. of Samples	Thickness of Slab, t (in.)	Width of Slab, w (in.)	Height of Slab (in.)
30	1-3/4	12	12

Circular-Core Circular Cylinder

No. of Samples	ID (in.)	OD (in.)	Sample Length (in.)
5	1.5	3.62	20
5	1.5	3.75	20
5	1.5	3.88	20
5	1.5	4.00	20
5	1.5	4.12	20
5	1.5	4.25	20
5	3.0	5.12	24
5	3.0	5.25	24
5	3.0	5.38	24
5	3.0	5.50	24
5	3.0	5.62	24
5	3.0	5.75	24

Table 12. (Continued).

Cross-Core Circular Cylinder*

No. of Samples	Width of Cross, 3ℓ (in.)	OD (in.)	Sample Length (in.)
5	1.5	3.62	20
5	1.5	3.75	20
5	1.5	3.88	20
5	1.5	4.00	20
5	1.5	4.12	20
5	1.5	4.25	20
5	3.0	5.12	24
5	3.0	5.25	24
5	3.0	5.38	24
5	3.0	5.50	24
5	3.0	5.62	24
5	3.0	5.75	24

*Shape of cross-core:  Each arm of cross is a square of side equal to ℓ

The test design adopted for critical-geometry testing of the rectangular samples will call for samples of constant thickness and length and varied widths to find the critical width for the given thickness. The theoretical prediction under these conditions is that

$$w_c = \left(\frac{x+1}{2x}\right)\sigma_c \tag{16}$$

where w_c is the critical width. From this equation it is clear that w_c is always greater than σ_c. The sensitivity of the critical-geometry tests is improved by using width as the variable, because it allows greater latitude in selection of size increments without jeopardizing the comparison with theoretical predictions.

Since w is the variable and x therefore is not constant it is necessary to use the following equation to determine the theoretically predicted w_c in terms of t and

$$w_c = \frac{t\,\sigma_c}{2t - \sigma_c} \tag{17}$$

In the hollow-core samples, the increments in OD are 1/8 in., which means that the increments in the web thickness will be 1/16 in. By the critical-geometry theory,

$$\text{critical web} = \frac{\sigma_c}{2} \tag{18}$$

so the increments are twice that used in testing for the critical side of a square column and the critical diameter of a solid cylinder. Smaller increments in the web thickness are beyond practical consideration. To match the 1/16-in. increments used in the solid cylinder and square column tests would require 1/16-in. increments in the OD of the hollow samples. Tube sizes are not available to meet such requirements economically.

3.3.3 Verification of Theory

The purpose of this subtask is to determine the validity of the critical-geometry theory by testing a material (AAB-3225) that has a critical diameter different from AAB-3189. Progress in this subtask must follow the satisfactory completion of Subtask 3.2.2, in which the critical diameter of AAB-3225 must be resolved, and it also awaits results from the critical-geometry tests to be performed in Subtask 3.3.2.

3.3.4 Initiation Pressure vs Pulse Width

The study of sensitivity to initiation of detonation customarily has consisted of Plexiglas card-gap tests. Data was acquired, under SOPHY I, on the card-gap sensitivity of AAB-3189. It is of further interest to investigate the amount of sensitivity of this material when subjected to an impulse of longer duration than that in Plexiglas, to determine whether the minimum shock pressure necessary to initiate a sample of a given diameter is affected.

This subtask will consist of tests in which the sensitivity of a super-critical-diameter sample of AAB-3189 will be tested either by the flying-plate technique or by an underwater technique such as that described by Liddiard (Reference 7). The former method is being analyzed at this time to determine its applicability to this test requirement.

3.3.5 Initiation Pressure vs Diameter

3.3.5.1 Test Objective

The purpose of this study is to determine the sensitivity of AAB-3225 propellant to initiation of detonation by the conventional Plexiglas card-gap method. A comparison with the sensitivity of AAB-3189 will provide qualitative information on the effect of RDX weight fraction on sensitivity, to allow a crude first estimate to be made of the sensitivity of unadulterated propellant.

As part of this subtask, supporting tests will be conducted to determine the shock wave-velocity attenuation history in the large diameters that will be used in the card-gap tests. The overall explosive weight of the boosters and acceptors that will be involved in these tests preclude camera documentation of the attenuating shock wave in the card-gap test itself. Separate attenuation measurements will calibrate the card-gap tests by relating the shock velocity and distance traveled in Plexiglas.

To determine the shock pressure of the wave entering the propellant, the Hugoniots of Plexiglas and AAB-3225 are required. The former is known. The latter must be determined experimentally. To do this, the method described in Reference 2 will be used. This involves the shock loading of a column comprised alternately of Plexiglas discs (1/4-in. thick, 1-in. diameter) and microtomed propellant wafers (nominally 0.1-in. thick). Streak camera coverage of the backlighted event will provide data on the shock velocity at each Plexiglas-propellant interface and the transit time through each propellant wafer. From these data it is possible to derive points on the propellant Hugoniot by the Hugoniot-reflection method (Reference 2).

3.3.5.2 Progress

Molds are being fabricated in diameters of 6, 7, 8, and 9 in. for samples to be cast from AAB-3225 propellant. When these samples are cast (requiring two 2000-lb batches), additional samples will be cast from the same batches to determine the critical diameter of each batch. These control samples will provide more data that is necessary to Subtask 3.2.2 in determining the critical diameter of this formulation.

Propellant wafers will be microtomed from surplus AAB-3225 propellant at Aerojet-Chino. Plexiglas discs with polished flats are being finished, and the Hugoniot test series will be performed in September.

3.3.6 Sensitivity of Unadulterated Propellant

3.3.6.1 Test Objectives

Since it is clearly impractical to conduct card-gap tests on supercritical, unadulterated, composite-propellant samples, and it is equally desirable that the sensitivity of this material be determined, a method

to estimate sensitivity by subcritical testing is required. In this subtask the objective is to evaluate the use of the axial resistance-probe technique as a means to arrive at the minimum critical shock pressure, P*, required to initiate detonation of adulterated propellant AAB-3189, and, if the technique does succeed, to determine P* for unadulterated propellant ANB-3226.

3.3.6.2 Background

3.3.6.2.1 Probe Performance

The axial resistance probe has been used for some time in the study of deflagration-to-detonation in high explosives (e.g., References 8, 9, and 10). The probes consist of a nichrome wire and copper wire, either cast in the sample parallel to, and equidistant from, the axis or wrapped one about the other to form a coaxial probe. The probe is shorted by the highly ionized medium immediately behind the shock front. As the detonation wave moves down the sample the resistance of the probe is reduced in direct proportion to the reduction in the length of the probe lying ahead of the shock front. The resistance probe is in a constant-current circuit, with the changing voltage being monitored on an oscilloscope. As the length of the probe ahead of the advancing wave diminishes, the resistance in the circuit diminishes, and since the current is held constant, the voltage in the circuit drops. The oscilloscope trace records voltage vs real time and, since the current level is known, the resistance vs time data are easily computed. Since the probe is made to a known resistance per unit length, it is a straight forward step to convert to distance-time data. The axial resistance probe thus supplies a continuous record of the behavior of the detonation wave at the axis.

3.3.6.2.2 Theoretical Basis for Application to Subcritical Sensitivity Testing

There are three major assumptions involved in the theoretical justification for applying the axial resistance-probe technique to subcritical sensitivity tests. First, the material near the axis of a subcritical cylindrical charge will not react differently from that in a supercritical or

ideal diameter charge until the effects of the incoming rarefaction regions are communicated to it. Experimental evidence obtained in SOPHY I during the testing of supercritical samples initiated by boosters that had diameters below the critical diameter of the acceptor (a nearly parallel example) showed such to be the case (Reference 2). In a test that resulted in failure to initiate detonation because the booster was too small, the detonation wave attenuation profile in the acceptor revealed that along the axis the wave was sustained at a constant velocity over the first diameter of the sample (4 in.). Finally, of course, the wave began to attenuate. The important fact is that momentary sustainment did occur, and at a velocity equal to the detonation velocity in AAB-3189 propellant.

The second assumption is that in the card-gap testing of a very subcritical sample, the small diameter will not reduce the time during which the velocity is sustained along the axis to an immeasureably small value. In the example cited above, the sample diameter was nearly 60% above d_c and the shockwave from the booster was not attenuated before reaching the propellant surface. Under these conditions, the sustainment lasted approximately 20 μsec.

The third assumption is that P*, the minimum shock pressure required to initiate detonation in an infinite-diameter sample, is not significantly different from the minimum shock pressure required to initiate chemical reaction in the material.

If the second assumption holds, one would expect to find a shock pressure above which the velocity stabilizes for a few microseconds and below which the velocity continuously decreases. In this event, determination of this pressure would be by noting the lowest pressure that produces a linear portion in the output of the probe. This pressure should be related to, or equivalent to P*.

If the third assumption is true, below P* there may be insufficient ionization produced to electrically short the probe, and the minimum pressure at which any pulse was generated could be considered as an estimate of P*.

3.3.6.3 Test Plan

Since the precise probe reaction will not be evident without some experimental data, the first step that will be taken is to test samples of AAB-3189, the formulation for which the initiation criterion was developed in SOPHY I. Using an axial probe in each subcritical sample, card-gap tests will be conducted at pressures above and below the P* estimated from the available data. The oscilloscope trace records will be studied to determine if any change in the voltage curve is repeatedly observed to occur at a specific and narrow pressure range. If a change is observed, that pressure below which the change occurs will be compared to the estimated P*. If the two values are comparable, the method will have been considered proven, and small (< 12-in. diameter) samples of ANB-3226 will be tested to determine the minimum pressure below which the same change is observed. That pressure will be considered to be a reasonably acceptable estimate of P* for ANB-3226.

3.3.6.4 Progress

The two types of probe design that are candidates for use in this subtask are the parallel-wire probe and the wrapped probe. The former consists of two copper wires and one nichrome wire placed near, and parallel to, the charge axis. The latter is made by wrapping the coated nichrome wire spirally around a heavier copper wire. The sensitivity of the wrapped probe is adjustable by the number of turns per unit length, and it is certainly greater than the sensitivity of the parallel-wire probe if the same size nichrome wire is used in each design. Greater strength can be built into a wrapped probe by using a larger diameter nichrome wire. A sensitivity greater than that of a 40-gauge straight wire (2 ohm/cm) is easily achieved with a 32-gauge wire wrapped around an 1/8-in. diameter rod.

The attributes of both designs, including cost, accuracy, sensitivity, and strength, are being evaluated at this time. Unless the wrapped probe is too costly to be produced in the small quantity required for this series, some samples will be cast with each probe for experimental evaluation.

3.4 LARGE CRITICAL-DIAMETER TESTS

3.4.1 Test Objective, Test CD-98

The large critical-diameter test program in SOPHY II was to experimentally determine the detonation behavior of unadulterated (ANB-3226) propellant, using the SOPHY I detonation model to select the appropriate test sample sizes. The SOPHY II test results are not intended to provide additional data for the SOPHY I model, since the test configuration is no longer an unconfined, single segment (Section 3.4.2).

The occurrence of a sustained detonation in the 72-in.-diameter test (CD-96) made the choice of diameter for the CD-98 test fairly simple. In a previous test, an unconfined 48-in.-diameter sample containing 0.25 weight percent RDX adulterant failed to sustain detonation (Reference 2). Assuming that this RDX content would at least have the effect on critical diameter that confinement by 0.080 aluminum has, which does seem to be a safe assumption, it would be concluded that a 48-in.-diameter unadulterated sample confined by 0.080 aluminum would fail to detonate. (The aluminum confinement is one requirement of the larger SOPHY II tests, to provide support for the mammoth grains.) The 60-in.-diameter chosen for CD-98 is midway between 48 in. (an implied NO-GO) and 72 in. (a verified GO).

3.4.2 Test Setup, CD-98

The test article consisted of a 60-in.-diameter by 240-in. high, four-segment solid-cylindrical propellant acceptor weighing 43,200 lb, and a 60-in. base diameter by 180-in. high, stacked, conical TNT booster that weighed approximately 10,700 lb.

The propellant sample was instrumented with T-2 targets, ionization probes, and ionization-mechanical probes to provide three velocity-measuring systems, each of which covered the full length of the sample. The progressive electrical shortings of the probes and T-2 targets were recorded on separate rasteroscillographs located in the control building.

The propellant sample was also fitted with an argon window, 6-in. wide, along the full length of the acceptor. A Beckman and Whitley streak camera recorded the event; the camera slit was lined up with the argon window to ensure sufficient luminosity to obtain a distinct streak record.

In the field, Kistler pressure transducers were mounted at gage stations along the three instrumentation legs to a distance of 1500 ft (Figure 9). Peak overpressure and impulse data were recorded from these blast gages.

The problem of obtaining reducible radiometer data had been studied during the weeks prior to this test; it was finally attributed to the fact that the radiometers were mounted in steel supported enclosures. Evaluation tests showed that the radiometers were very effective when they were shock mounted in a simple wooden stand. This radiometer mount design isolates the detector from the severe high frequency vibrational waves, which can be transmitted to it by a steel structure. The excessive noise on the records, such as those produced in the 72-in. diameter test, originated from the steel support.

Photographic coverage from the ground included (1) 16mm cameras, using color film, running at framing speeds of 64, 400, 1000, 4000, and 8000 fps; (2) a 35mm camera running at 6 fps; and (3) an infrared sensitive film in a camera operating at 400 fps. Helicopter-borne coverage of the event was cancelled because the helicopter encountered stability problems. Documentary coverage of the event, using a 16mm camera located 1-3/4 miles away from the test site, used color film run at 50 fps.

A steel plate, 10 ft square by 1/2 ft thick, was used as the witness plate. As in the 72-in. diameter test (Reference 11), a concrete box which supported the plate along its edges allowed an air gap beneath that portion of the plate upon which the 60-in. diameter sample rested.

3.4.3 Test Results, CD-98

3.4.3.1 General Observations

High-speed cameras recorded, and eyewitnesses observed, that many burning propellant fragments were thrown off by the 60-in.-diameter sample. The propellant fragments were thrown to a distance of 2500 ft,

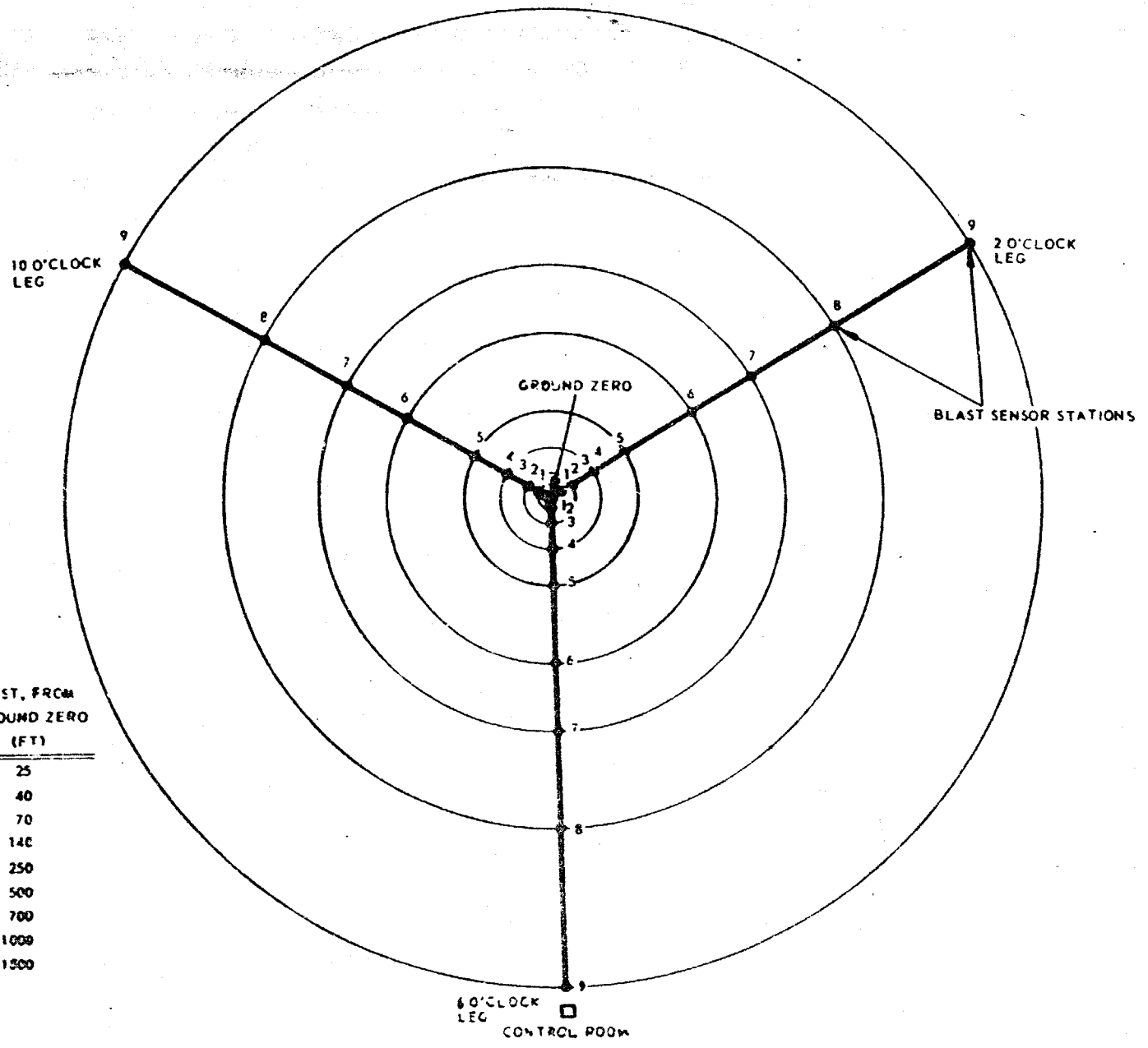

STATION NO.	DIST. FROM GROUND ZERO (FT)
1	25
2	40
3	70
4	140
5	250
6	500
7	700
8	1000
9	1500

Figure 9. Blast Instrumentation Legs, AFRPL 1-36D Facility.

and appeared to emanate from the lower third of the charge. The trajectory of most of the fragments from a distance appeared to be nearly horizontal, a few large chunks were sent high in the air. Burnt propellant and burning brush were in evidence throughout the test area.

Large pieces of the aluminum restraint fixtures were recovered, some as large as 4 ft by 1 ft. Their size was typical of that expected from a nondetonation.

The witness plate was in position at ground zero, resting on a slight mound. The plate was slightly dished, but bore no sign of indentation, and it was intact except for the loss of the lifting lugs that had been welded upright at the corners.

The detonation-velocity data obtained from three sets of probes, each different, and from the streak camera record, are shown in Figure 10. The rate of attenuation of the velocity is more gradual than has been observed in most NO-GO tests, but the data do agree with the expected behavior of an attenuating wave near the hydrodynamic sound velocity. This matter is discussed further in Section 3.4.4.

Peak overpressures from the 60-in. test are shown against a series of Kingery TNT curves in Figure 11. These overpressure data are tentative, awaiting calibration of the blast instrumentation. For comparison, the 72-in. diameter peak overpressure data are shown in Figure 12. The two sets of data are also presented in Table 13.

The radiometer data, measuring the thermal flux at 400 ft and 500 ft ranges reduced to a maximum flux of 3.5 w/cm^2 at the near station and 2.5 w/cm^2 at the far station. These fluxes represent the level incident on the radiometers at the distances and are not meant to be estimations of the radiation flux at the fireball surface. Both radiometers recorded the pulse duration to be 6.5 sec.

3.4.4 Interpretation of SOPHY II Critical-Diameter Data

3.4.4.1 SOPHY I Criteria

In the SOPHY I critical diameter program (Reference 2) the nature of the detonation velocity-distance curves obtained from pin-probe and streak-camera data and the effects of the steady-state or fading detonation waves on steel witness plates were used to classify the detonation

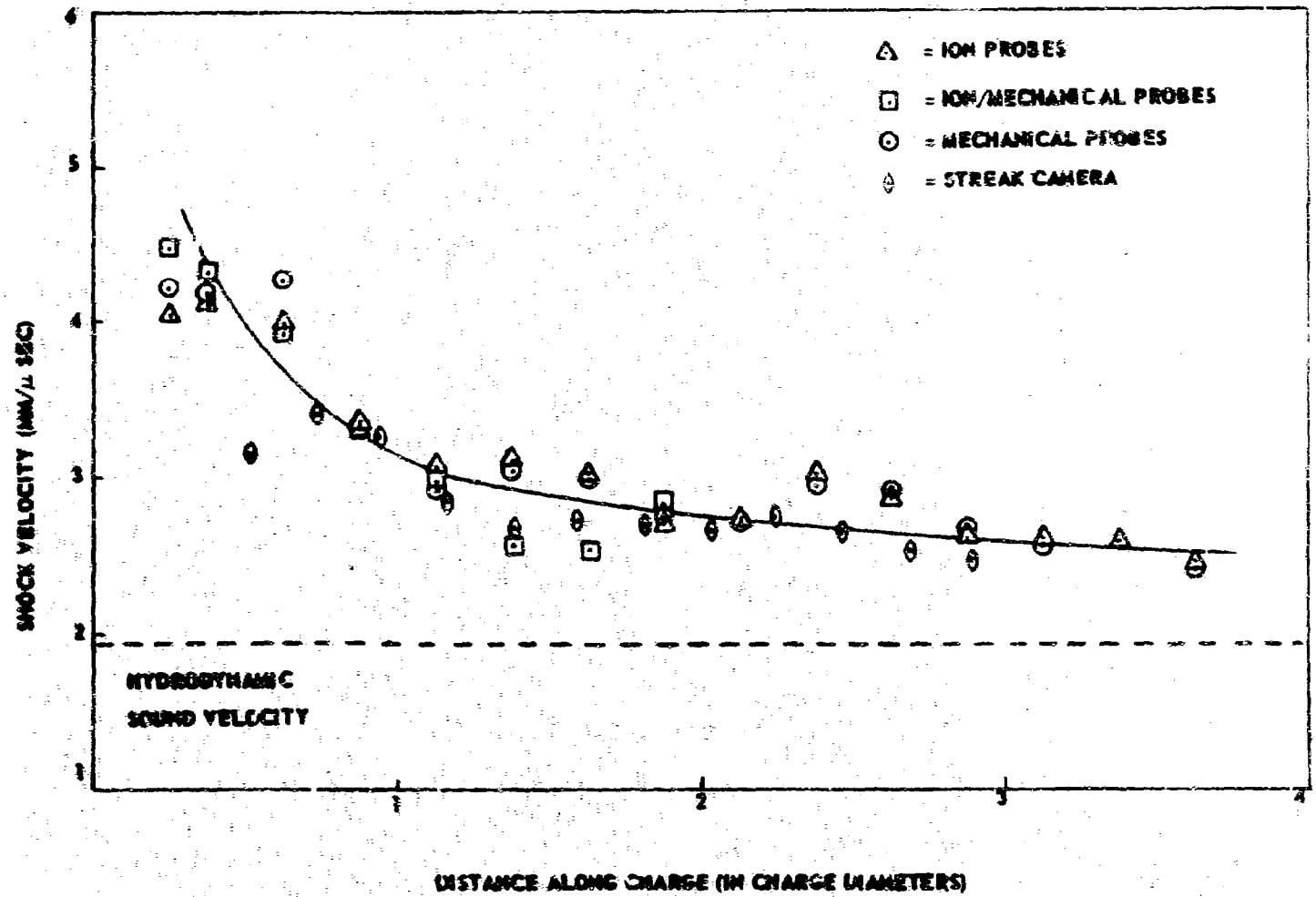

Figure 10. Detonation Velocity vs Distance, Task CD-98.

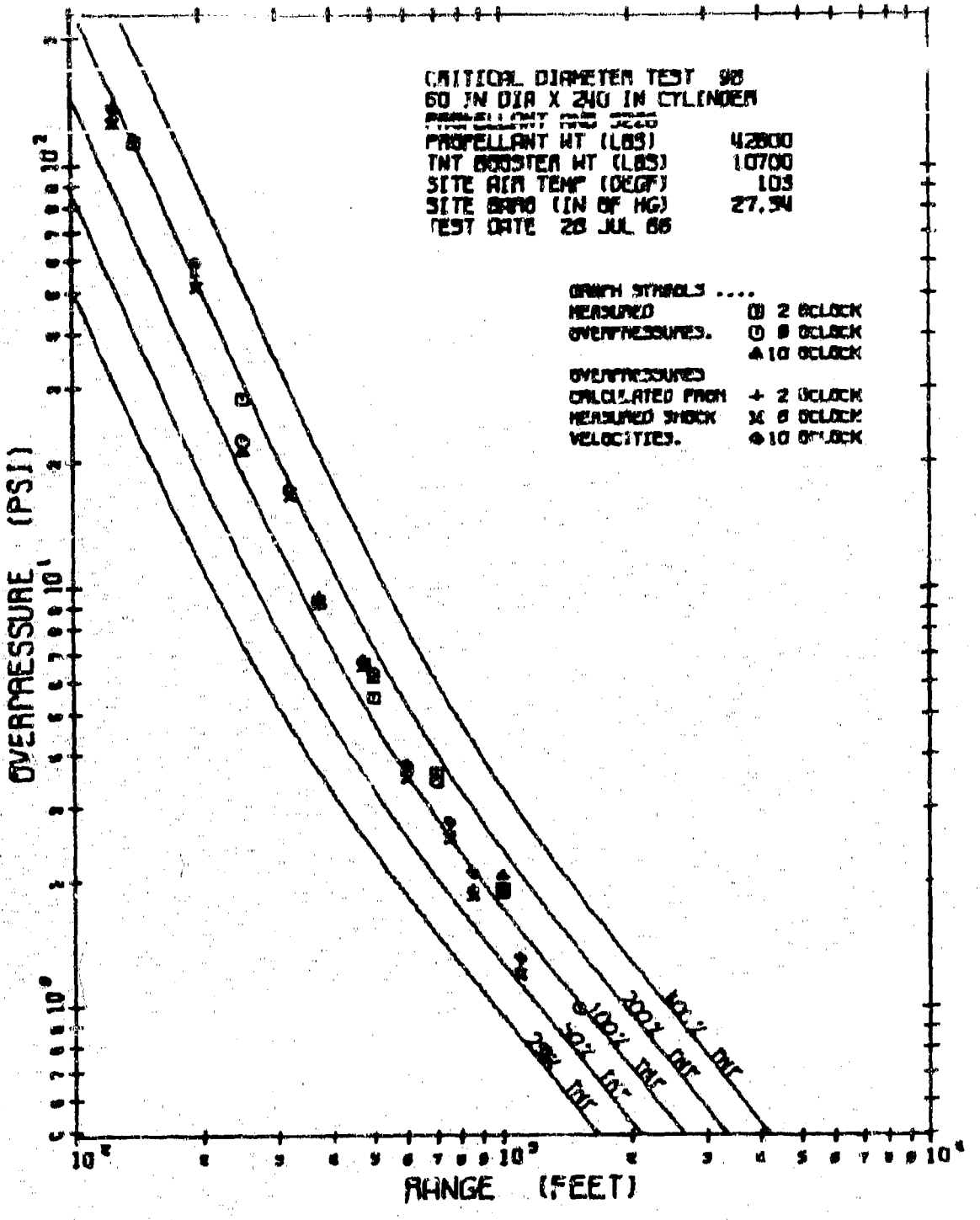

Figure 11. Peak Overpressure Data from 60-in. Test.

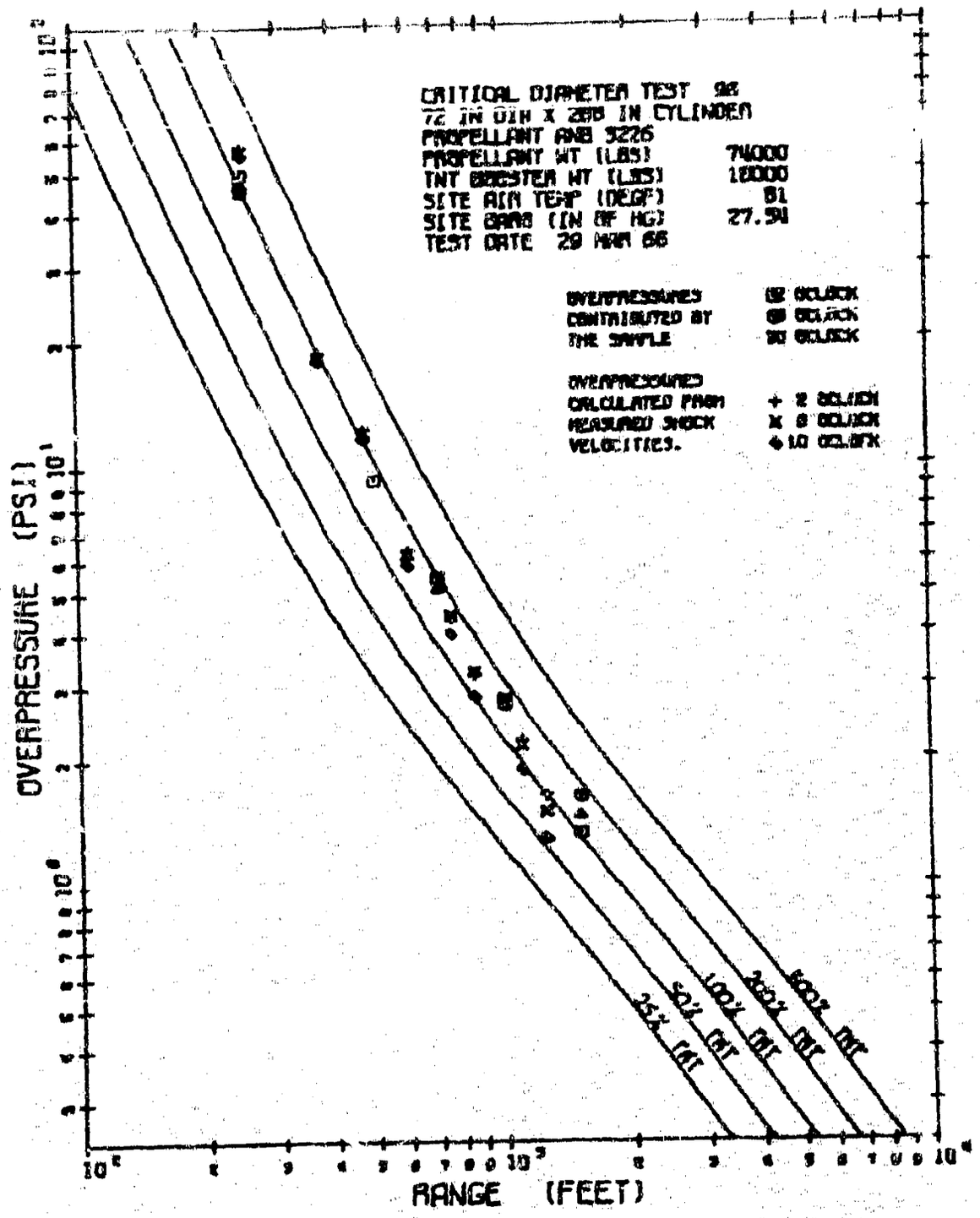

Figure 12. Peak Overpressure Data from 72-in. Test.

Table 13. Observed and Calculated Side-On Overpressure and TNT Equivalences in the 72-in. and the 60-in. Critical Diameter Tests.

(IMPORTANT: The data presented in this table are preliminary. Their values are subject to change pending further reduction and analysis.)

Radial Distance from Charge (ft)	Radial Direction (o'clock)	Peak Side-on Overpressure† Measured (psi)		Peak Side-on Overpressure† Calculated (psi)		TNT Equivalence From Measured Overpressure (%)		TNT Equivalence From Calculated Overpressure (%)	
		72-in. Test	60-in. Test	72-in. Test	60-in. Test	72-in. Test	60-in. Test	72-in. Test	60-in. Test
140	2	**	125	-	-	**	199	-	-
	6	**	**	-	-	**	**	-	-
	10	**	126	-	-	**	201	-	-
250	2	54.0	31.0	-	-	223	177	-	-
	6	50.3	25.4	-	-	208	129	-	-
	10	*	24.2	-	-	*	120	-	-
375	2	**	**	20.2	10.7	**	**	193	128
	6	**	**	19.9	10.4	**	**	188	121
	10	**	**	19.6	10.4	**	**	184	121
500	2	10.1	6.12	-	-	155	124	-	-
	6	*	6.90	-	-	*	157	-	-
	10	**	6.68	-	-	**	147	-	-
600	2	**	**	6.81	4.11	**	**	136	103
	6	**	**	6.71	3.98	**	**	131	95
	10	**	**	6.35	4.24	**	**	128	110
700	2	5.82	3.91	-	-	177	160	-	-
	6	*	3.74	-	-	*	145	-	-
	10	5.51	3.79	-	-	151	150	-	-
1000	2	2.98	2.09	-	-	132	127	-	-
	6	2.90	2.05	-	-	126	121	-	-
	10	2.95	2.22	-	-	130	149	-	-
1500	2	1.45	**	-	-	92	**	-	-
	6	1.72	1.09	-	-	145	91	-	-
	10	1.57	**	-	-	115	**	-	-

† Measured overpressures are derived from Kistler transducer measurements. The calculated overpressures are calculated at midpoint distances between Kistler transducer stations from which time-of-arrival data are available. The calculations are performed using an equation derived from the Rankine-Hugoniot equations:

$$p = \frac{2\gamma}{\gamma + 1} P_o \left(\frac{U^2}{c_o^2} - 1 \right)$$

where, p = peak overpressure on the shock front
γ = ratio of specific heats for air
P_o = test-site atmsopheric pressure
U = velocity of shock front
c_o = sound velocity at test site

*No data, because of gauge failure.
**No side-on overpressure gauge placed at this location.

behavior of RDX-adulterated propellant samples as supercritical or subcritical. Samples whose velocity-distance curve became essentially horizontal after the initially overdriven wave had propagated about halfway along the charge, and which either punched the witness plate or produced definite metal flow, were considered supercritical. If the wave velocity showed a nearly continuous decrease along the entire length of sample, and if the witness plate was intact and either dished or undamaged, the sample was considered subcritical.

These criteria clearly distinguish between supercritical and subcritical behavior in a material if the steady-state detonation velocity is (1) high enough to transmit a sufficiently strong shockwave to the steel witness plate to punch it or cause metal flow, and (2) is sufficiently above the hydrodynamic sound velocity so that the fading detonation wave in a subcritical sample will not fade so slowly that its velocity-distance curve is undistinguishable from that of a supercritical sample. In the SOPHY I tests, although the steady-state velocity at the critical diameter was found to decrease with decreasing RDX content, the value for the samples of lowest RDX content was high enough so that all of the critical diameter data could be interpreted in terms of the criteria as originally formulated.

In the course of the SOPHY I program two phenomena were noted which correlated perfectly with the velocity-distance and witness-plate criteria, and which could serve as supplemental criteria for classifying detonation behavior. First, it was noted that the witness plates from GO reactions with propellants of low RDX content were extensively broken up while those from NO-GO's were dished but intact. Second, examination of the documentary and Fastax films showed that in all of the tests that were classified as NO-GO's by the velocity-distance and witness-plate criteria, pieces of burning propellant were expelled laterally from the charge. No burning propellant could be detected in the film records of the GO's.

3.4.4.2 Analysis of SOPHY II Test Results

The two SOPHY II large-critical-diameter test sizes (72-in. and 60-in. diameter) were chosen to give a GO and a NO-GO reaction with unadulterated propellant, according to predictions of the model (Reference 2). In terms of the supplemental criteria developed in the SOPHY I

program, the 72-in. diameter test was an unequivocable GO and the 60-in. diameter test was an unequivocable NO-GO, i.e., in the 72-in. diameter test, no burning propellant could be detected in the documentary and Fastax film records, and the witness plate was extensively fractured; in the 60-in. diameter test, considerable burning propellant was ejected from the charge and the witness plate was dished out unbroken. A cursory examination of the velocity-distance data showed that the curves for the two tests were quite similar (Figures 10 and 13), confirming an earlier conjecture that at sufficiently low critical detonation velocities, there might be no apparent differences between subcritical and supercritical curves.

Because of the similarity between the D vs x curves for the 72-in. and 60-in. diameter tests it has been necessary to examine them in greater detail in order to use them to classify the tests as supercritical or subcritical. For this purpose, both curves have been compared with D vs x data for a subcritical sample of an aluminized AP-PBAN propellant sample of similar composition (Reference 11) and with data for the attenuation of an unreactive shock in Plexiglas (Reference 12). The data for Plexiglas are shown in Figure 14, where the observed velocity is plotted vs the reduced distance, x/d, that the shock wave has progressed into the Plexiglas. (Although the data are for a 0.5-in. Plexiglas column, a previous, unpublished analysis indicates that the plot of shock strength vs x/d is nearly identical for Plexiglas columns with diameters varying by a factor of 12.)

It is apparent from this plot that even in the case of a nonreactive shock, the rate of decay is so gradual at x/d = 4 that the curve appears essentially flat, although still appreciably above its hydrodynamic sound velocity. Had the material been a propellant instead of Plexiglas, the original D vs x criterion would have classified the behavior as supercritical.

In Figure 15 the data for the 72-in. and 60-in. diameter tests are compared with that for Plexiglas and the data for a subcritical (22-in. diameter) sample of aluminized AP-PBAN propellant. The velocity data for the three propellant samples is expressed as the difference between the observed velocity and the (estimated) hydrodynamic sound velocity (assumed to be the same as that previously determined for RDX-adulterated propellant containing 9.2 weight percent RDX, i.e., $\sim$ 1900 mm/μsec (Reference 2).

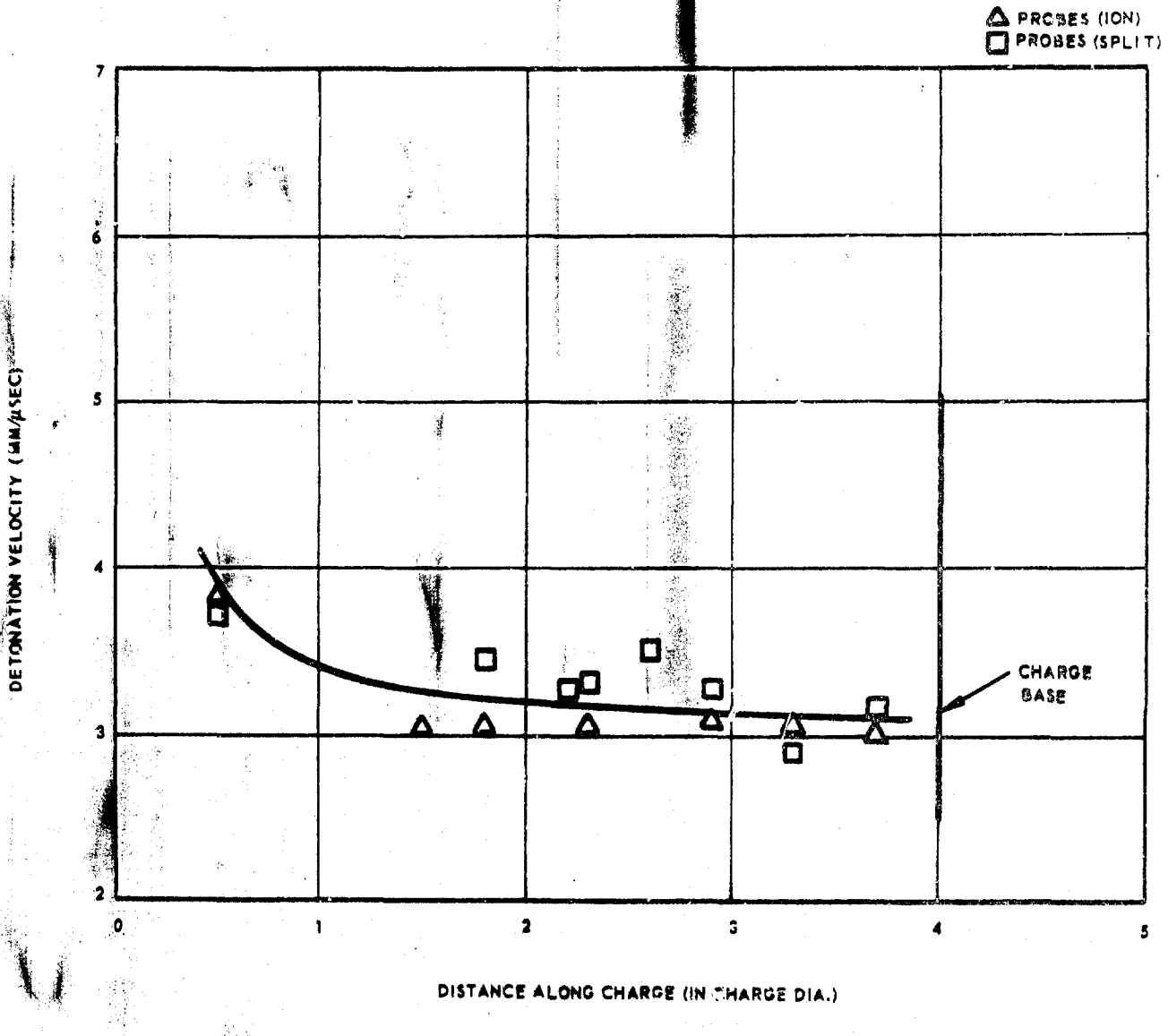

Figure 13. Detonation Velocity vs Distance Along Charge.

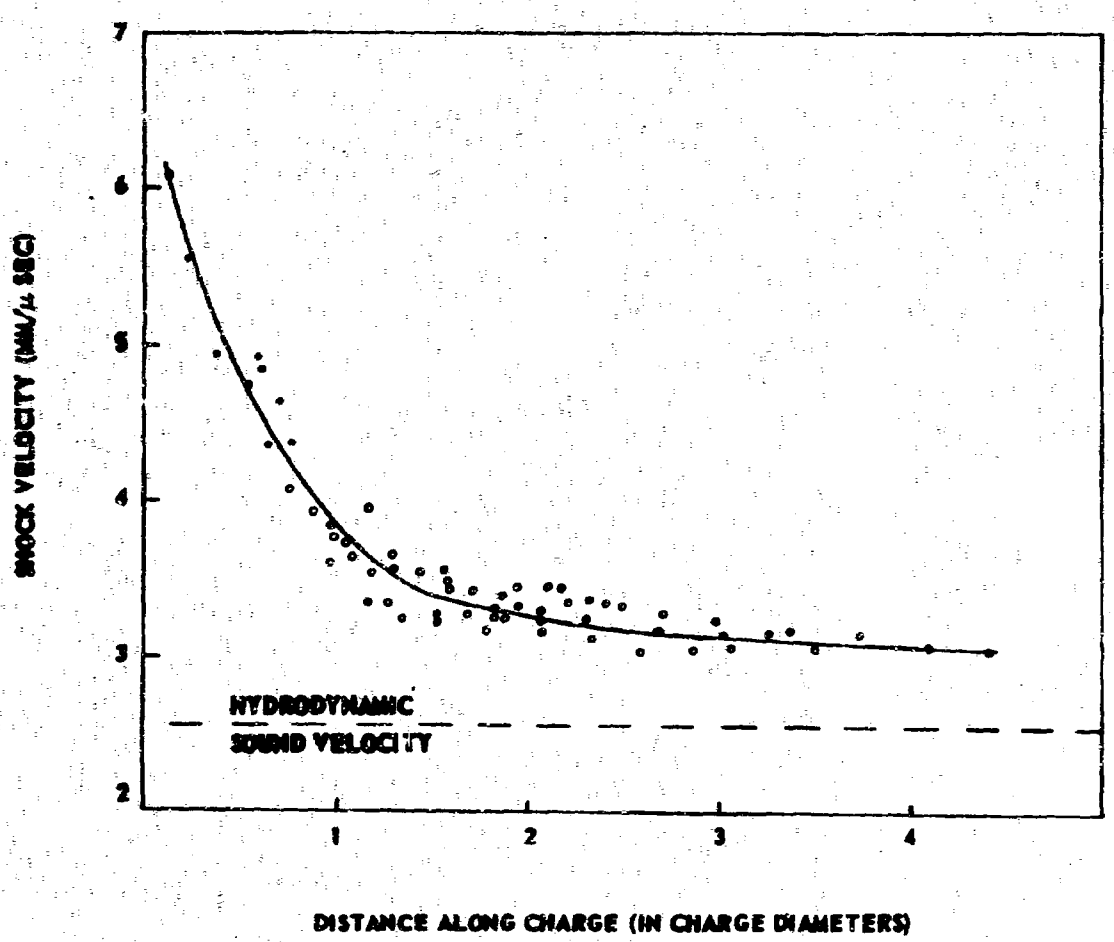

Figure 14. Shock Attenuation in Plexiglas.

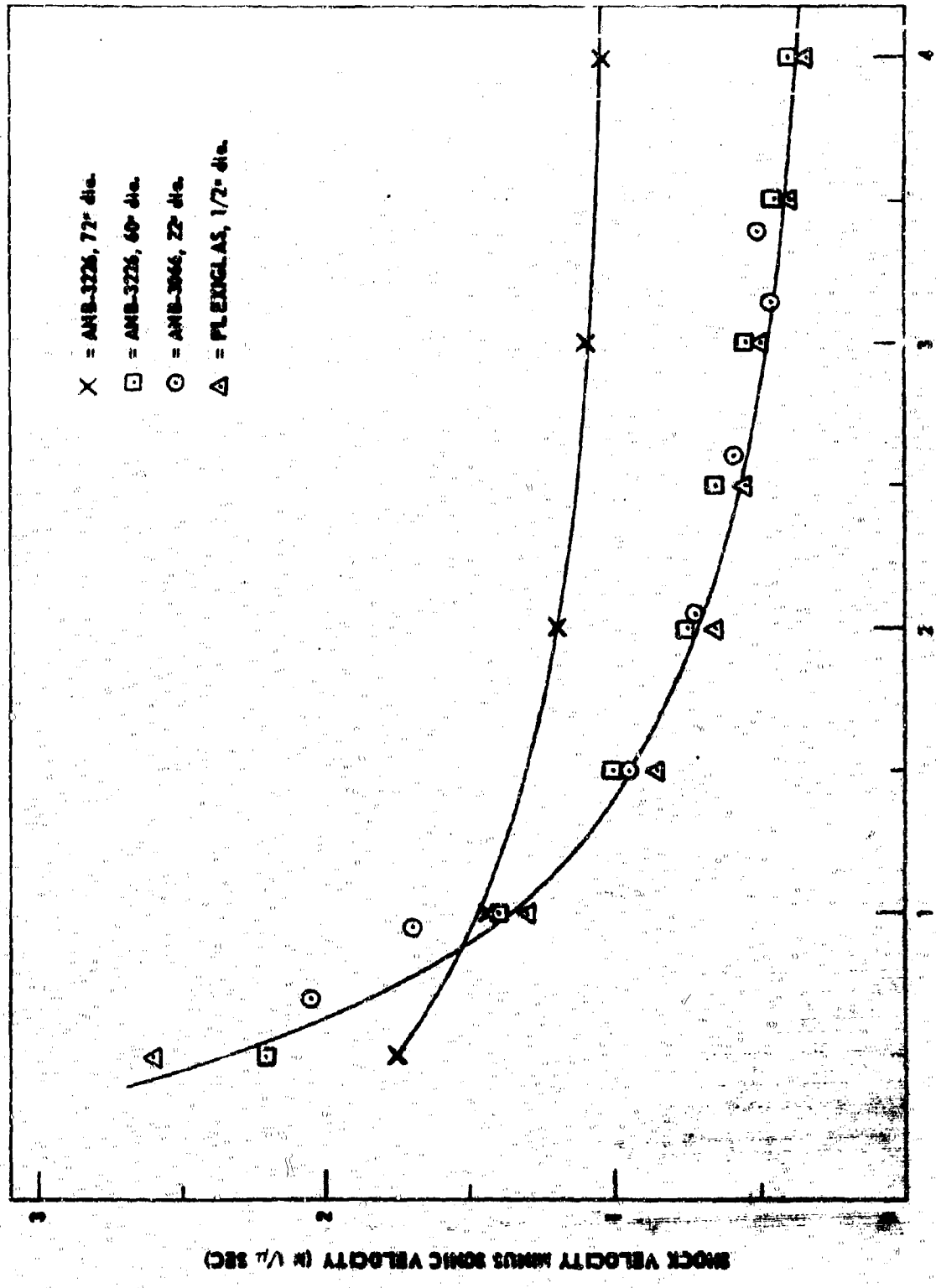

Figure 15. 72-in. and 60-in. Test Data Compared with Data from Plexiglas and AP-PBAN Propellant.

The comparison of Figure 15 indicates that the D vs x curve for the 60-in. diameter test closely follows the curve for the subcritical (22-in. diameter) test and the curve for the attenuation of an unreactive shock in Plexiglas. The curve for the 72-in. test, however, is distinctly different. It approaches a steady-state velocity (~3200mm/μsec) which is considerably above that reached in the nonreactive curves at the same position (x/d = 4). The 60-in. test is therefore judged subcritical and the 72-in. test supercritical, in agreement with the clear-cut classification by the supplemental criteria.

This analysis clearly demonstrates that the approach of a detonation wave to an apparently steady-state value somewhat above the hydrodynamic sound velocity is not adequate evidence of supercriticality when the critical velocity of the composition is near its hydrodynamic sound velocity. In the present case, consideration of this data in conjunction with the other evidence has permitted a clear distinction to be made.

3.4.5 Fireball Data, CD-96 and CD-98

The 72-in. diameter test (CD-96) and the 60-in. diameter test (CD-98) were recorded by a number of high-speed cameras. The films were read for fireball diameter and height. The data were finally plotted as fireball growth, over the first 100 msec, and fireball size history, during the first 5 sec. Fireball diameter is taken to be the maximum horizontal dimension of the fireball; fireball height is the maximum vertical dimension of the fireball, not the height of the fireball above ground. That is, when the fireball lifts off the ground, height becomes the vertical diameter of the fireball.

The fireball growth in CD-96 is shown in Figure 16. Only the fireball diameter is graphed, because all the cameras had the charge so high in the frame that the top of the fireball was very quickly out of frame, which prevents height measurement. Excellent agreement is seen to have been reached in the films taken at camera stations F and G. Other records are not reducible, either because of (1) poor focus, (2) too great a range of camera speed from the beginning of the event to the end, or (3) because the posts near the charge, which are used to obtain a distance-scaling factor, were not detected in the film.

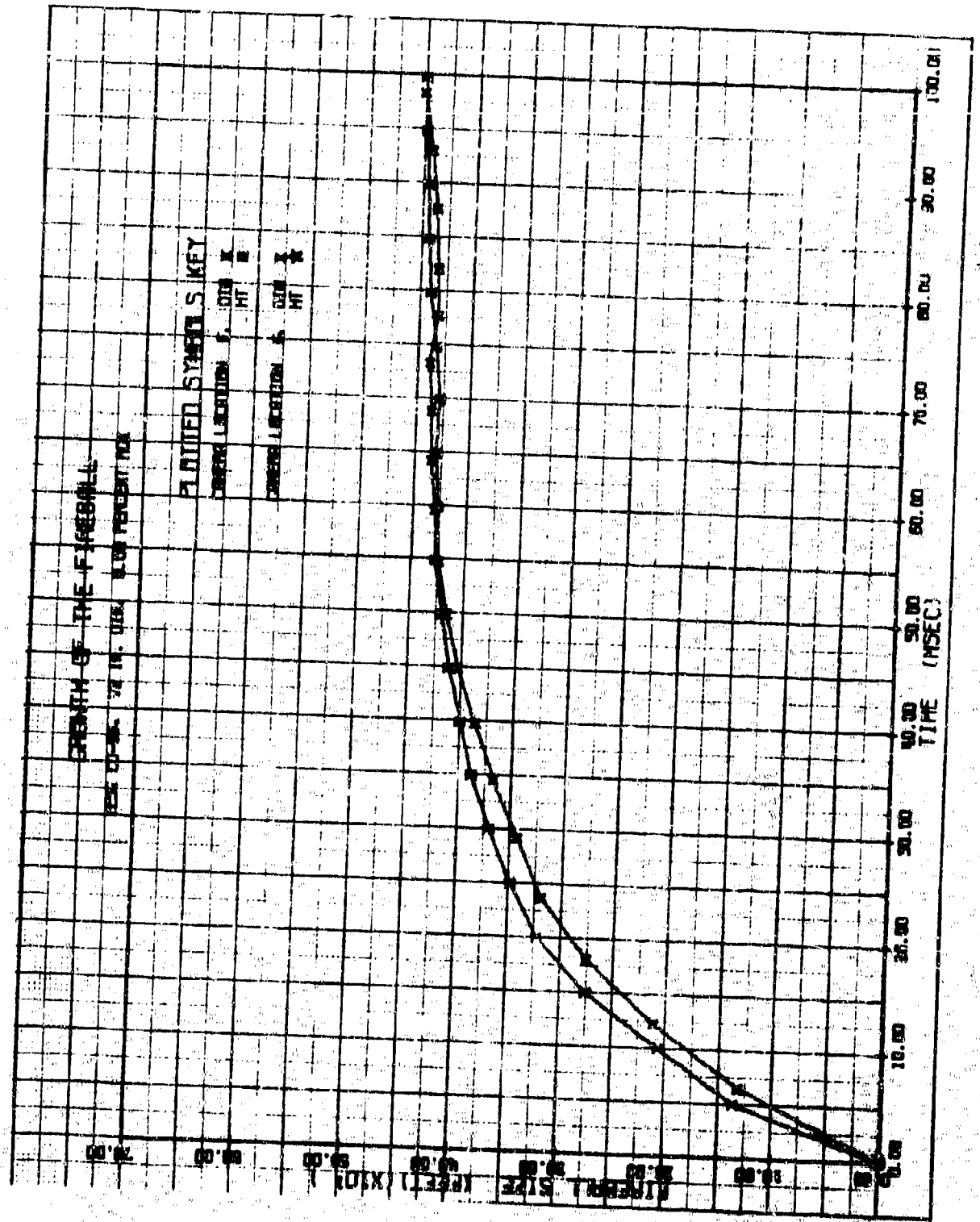

Figure 16. CD-96 Fireball Growth.

The fireball history in CD-96 is shown in Figure 17. The short duration of the information is again a result of poor framing.

The CD-98 fireball growth, from the film taken at camera position D, is shown in Figure 18. The "spikes" at the very start of the curves are the measurement of the initial flash size. The fireball history, plotted in Figure 19, shows the fireball had a total duration time of 4.25 sec, a maximum diameter of 410 ft and a maximum height of 345 ft.

3.5 PROPELLANT DEFECTS STUDY

3.5.1 Task Objective

In the interest of developing capability in producing controlled defects in composite propellant and developing methods by which the defects can be analyzed, the Research and Technology Operations of Aerojet's Sacramento Plant has begun a development study that has the following objectives:

a. Attempt to synthesize uniformly-porous propellant having average pore sizes of (1) 0.1 - 1mm diameter and (2) near 10μ diameter.

b. Synthesize the material in (a) to 5 - 10% and 20 - 30% porosities.

c. Prepare cracked grains having approximate surface area per unit volume of 10 - 15 cm^2/cm^3 and 40 - 50 cm^2/cm^3.

d. Develop techniques to characterize defective propellant made in sections (a) - (c).

3.5.2 Progress

The major effort has been directed to the production and characterization of unconnected pores in ANB-3226 propellant. Fourteen 10-lb batches have been prepared.

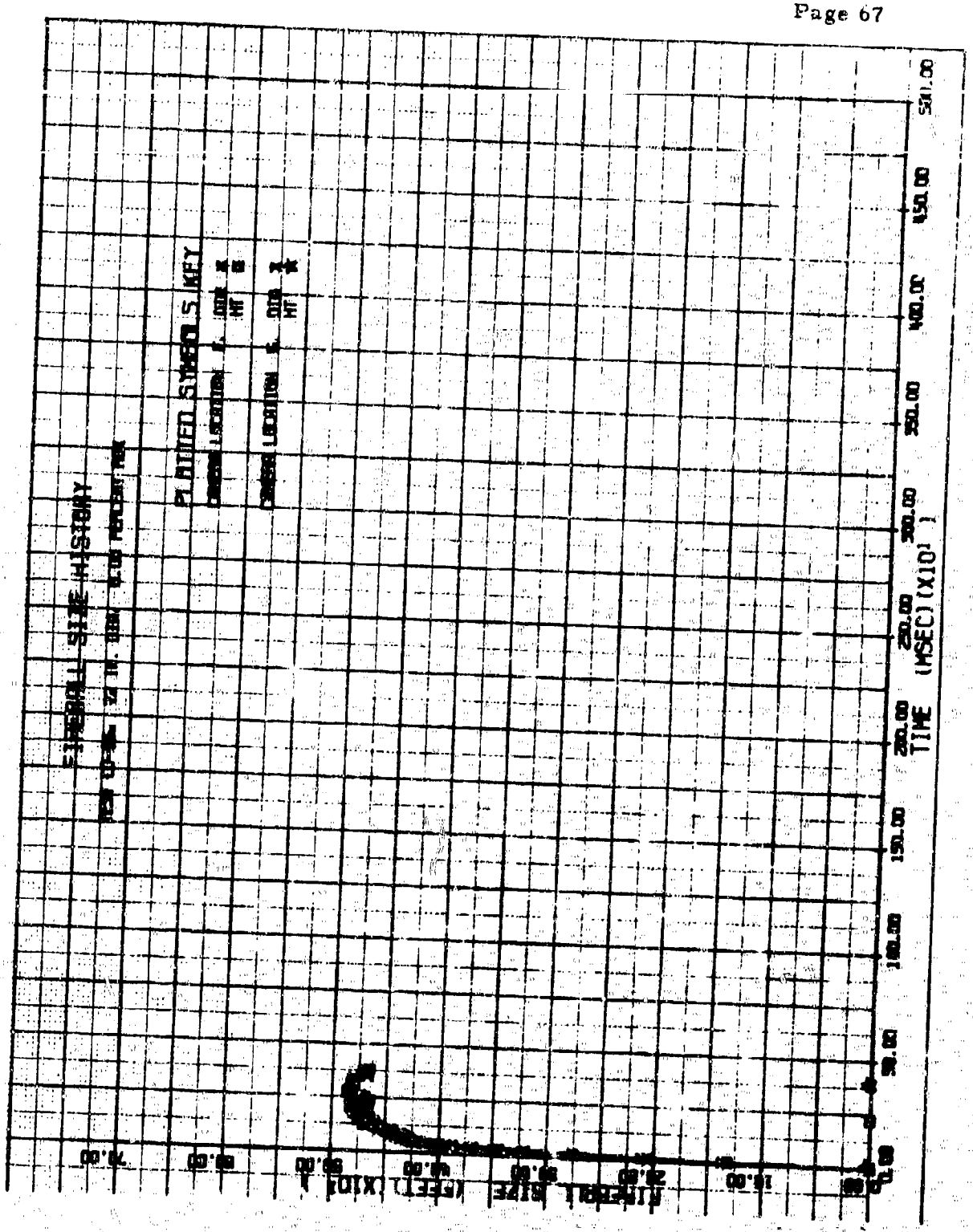

Figure 17. CD-96 Fireball History.

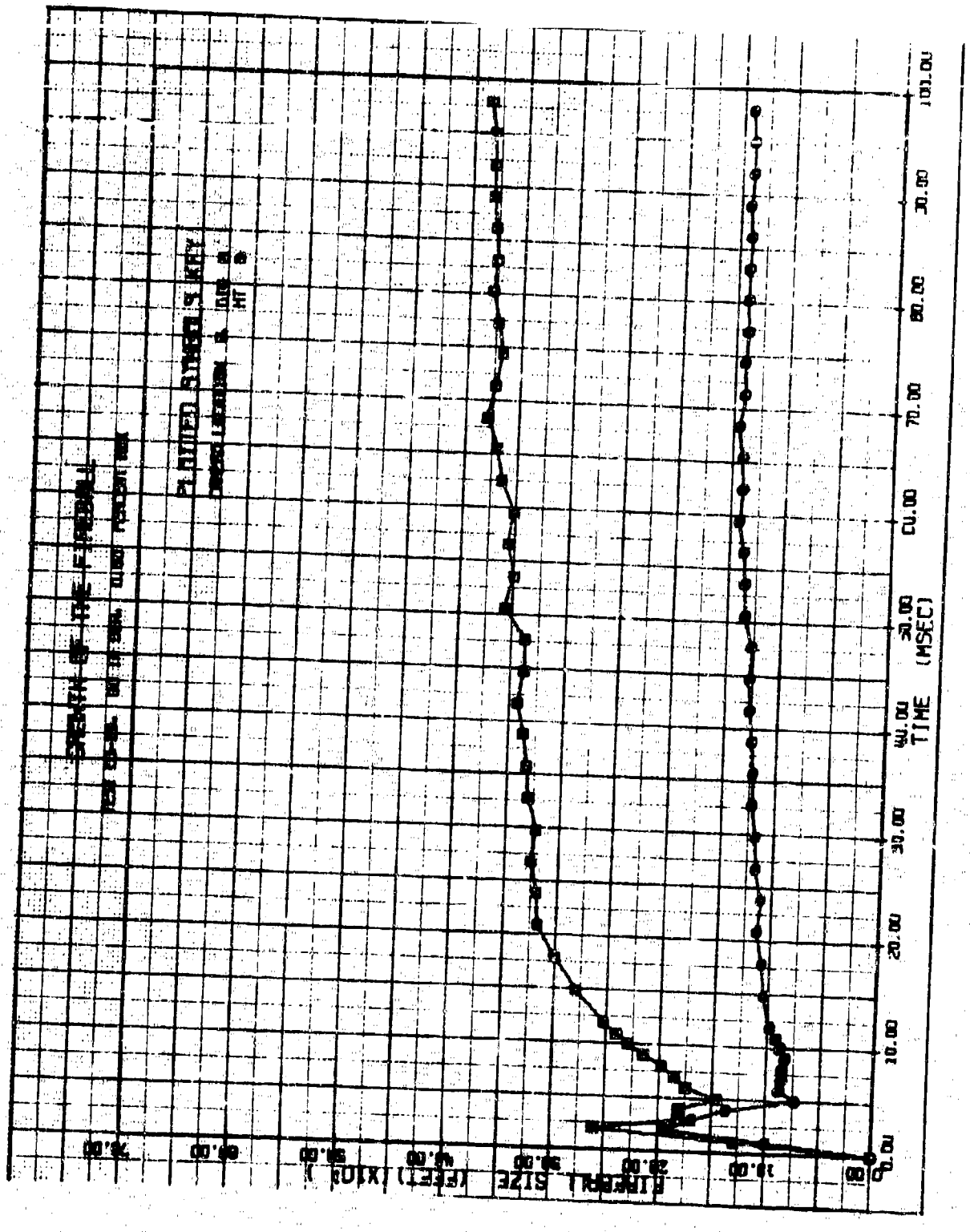

Figure 18. CD-98 Fireball Growth.

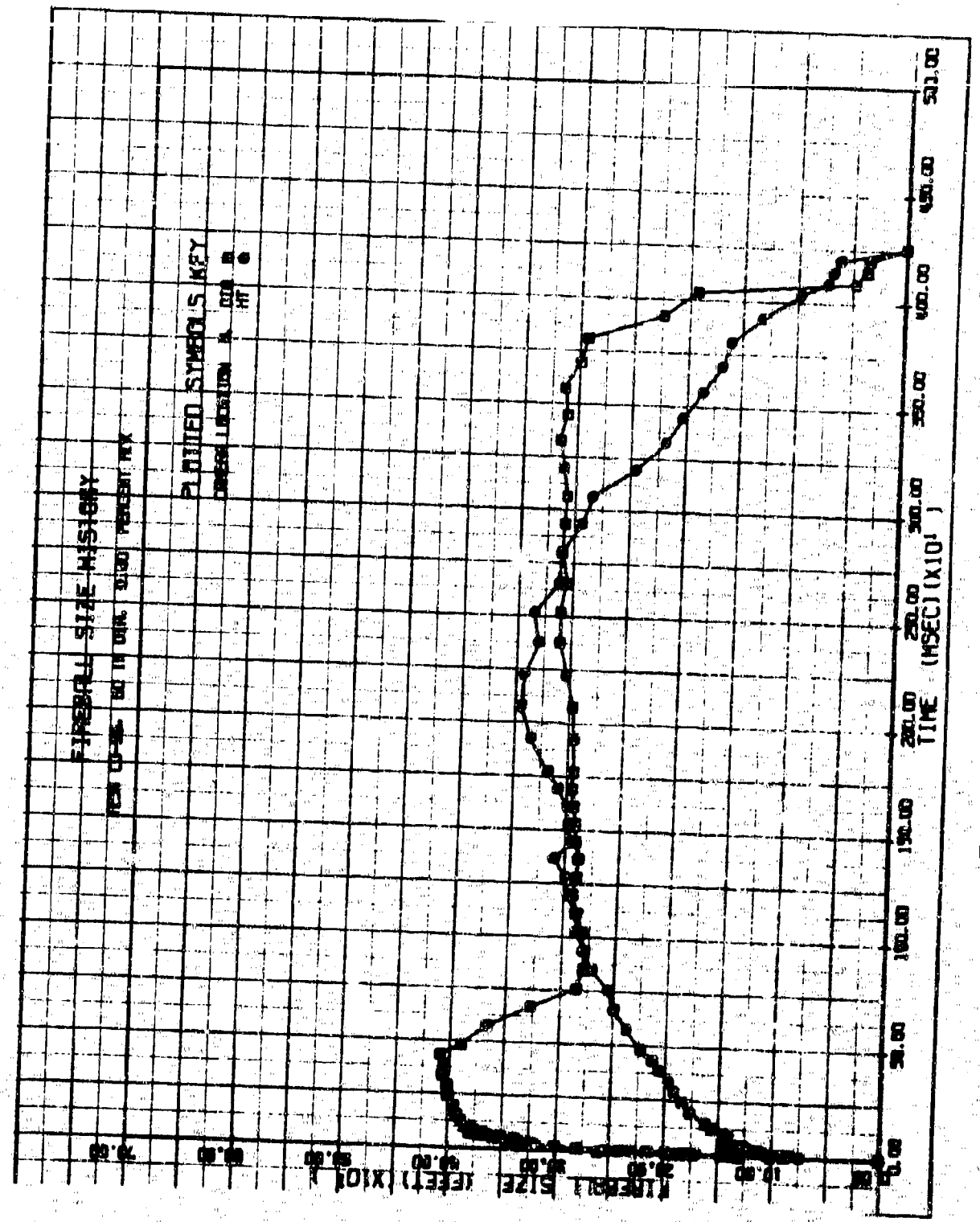

Figure 19. CD-98 Fireball History.

In two batches, the binder ingredients, excluding diepoxide resin (DER), were preblended in beakers and subjected to 3 hr of gas entrainment by bubbling extra-dry nitrogen through the binder at a flow rate of 55.5 ml/sec. One binder was held at 130°F and the other at 77°F during the nitrogen adsorption period. Both batches were mixed at 135°F without vacuum and vibrated for a short period to bring the air entrapped during mixing to the surface.

Six 3 by 5 by 1-in. plastic containers were cast from each batch. Two containers from each batch were cured at each of three temperatures: 110, 135, and 150°F. This was done to determine whether the adsorbed nitrogen in the binder would be affected by the cure temperature. As expected, the propellant cured at 135 and 150°F cured to Shore "A" hardness values of 28 to 34 in 1 week. The samples cured at 110°F for 1 week were placed at 135°F for an additional 1-week cure cycle. Samples from the four plastic containers cured at the higher temperatures were examined microscopically; densities of these will be determined to establish the total porosity.

Preliminary microscopic examination indicates that pores of varying size within the desired range (0.1 to 1mm diameter) were achieved and their distribution was affected both by nitrogen adsorption in the binder and the temperature of cure.

In the next six batches the binder ingredients (excluding the DER) were Cowles dissolved at 2400 rpm under a nitrogen blanket to achieve complete homogeneity of the binder. In order to remove the nitrogen worked into the binder by Cowles dissolving, the binder was degassed at ambient temperature for 6 hr at 29 in. of Hg vacuum. A study of the gas entrainment into a degassed binder was accomplished with standard laboratory gas flowmeters and heating mantles. The change in viscosity with temperature was measured with a Haake rotoviscometer and is shown in Figure 20. These data indicate that an appreciable change in viscosity occurs between 80 and 140°F. This change in viscosity is useful in the production of various size nitrogen bubbles in this binder. At ambient temperature (77°F) nitrogen bubbles of approximately 1mm are produced. The size distribution of these bubbles at this temperature is in a very narrow range. At 140°F the production of very small bubbles takes place. A variation in the gas flow rate at ambient temperature from 13.5 ml/sec to 55 ml/sec produces a marked change in the number of gas bubbles. At 55 ml/sec numerous bubbles are produced. However, at 13.5 ml/sec flow rate, a significantly smaller number of bubbles is formed. This effect of difference resulting from gas flow is not present at 140°F.

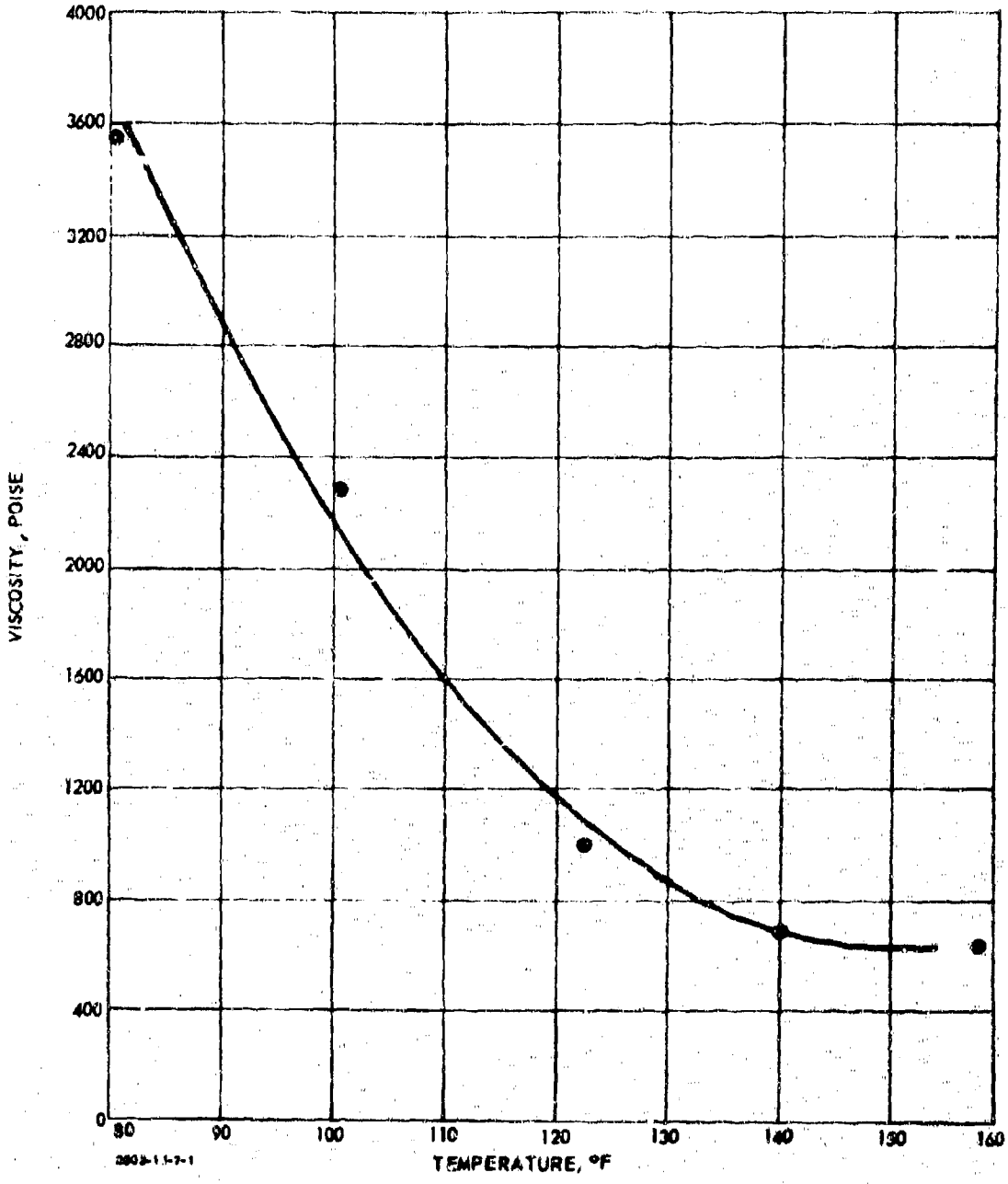

Figure 20. The Effect of Temperature on the Viscosity of ANB-3226 Binder.

The six batches of ANB-3226 propellant were made without vacuum according to the following test plan:

Batch No.	Binder Temperature (°F)	Gas Flow Rate (ml/sec)
1	140	25
2	77	25
3	77	55
4	77	10
5	140	55
6	140	10

This test plan allowed test of variation in temperature of the binder with the gas flow held constant and variation of the gas flow with the binder temperature held constant. Three 3-in. by 5-in. by 2-in. plastic containers were cast from each batch and cured at 110, 135, and 150°F. These samples were trimmed. The density data with the test plan and processing variables used are presented in Table 14. The first set shown on the table indicated that the density of the propellant was significantly decreased by maintaining a high submix temperature during aeration. However, the second test set, in which flow rate was added as a variable, showed that the only significant factor causing a change in the propellant density was the cure temperature; as the cure temperature increases the propellant density becomes greater. Although these significant effects were observed, the resulting void percentages are far too low and the noted effects may disappear when processes are found to produce higher void percentages.

The microscopic study of voids is being performed at two magnifications: (1) macrophotography of block sample, and (2) microscopic examination of microtomed thin sections at 125X. From examination of photographs of Set 1, it was seen that the aeration at the highest temperature resulted in the smallest voids with the most uniform distribution. No difference in cure temperature could be seen. From photographs of Set 2, the difference in cure temperature was easily visible; the low temperature cure samples had more voids. The other processing differences, flow rates

Table 14. The Solid Density of ANB-3226 Propellant Prepared from Aerated Binder.

Set*	Batch No.	Binder Temperature During Aeration (°F)	Gas Flow Rate (ml/sec)	Cure Temperature (°F)	Propellant Solid Densities (gm/ml)	Average	Voids (%)
1	6416	140	25	110	1.6305		
		140	25	135	1.6371	1.6361	5.5
		140	25	150	1.6406		
	6417	77	25	110	1.6484		
		77	25	135	1.6589	1.6545	4.5
		77	25	150	1.6601		
2	6613	140	55	110	1.6477		
		140	55	135	1.6533	1.6522	4.3
		140	55	150	1.6556		
	6614	140	10	110	1.6464		
		140	10	135	1.6532	1.6501	4.5
		140	10	150	1.6507		
	6534	77	55	110	1.6457		
		77	55	135	1.6573	1.6537	4.8
		77	55	150	1.6571		
	6535	77	10	110	1.6426		
		77	10	135	1.6496	1.6495	4.5
		77	10	150	1.6564		

*Set 1 samples cast without vibration.
Set 2 samples vibrated after casting.

and binder temperature, could not be seen from the photographs. Microscopically, the smallest voids in all the samples are the same and measure about 0.10mm diameter. The voids range to 1mm in size with a few in some cases up to 3mm.

Work is in progress to develop a method for the statistical evaluation of the void content of the samples from microscopic examination. A line-intercept method has been devised for this study which will permit evaluation of samples found to be homogeneous enough for counting of void distributions.

Six additional batches of 10-lb batch size were prepared to study submix aerated with nitrogen during Cowles dissolving but not subsequently degassed and reaerated as with previous binders. (Submix contains all binder ingredients except DER, the diepoxide curing agent.) Submix sufficient for the preparation of two batches was master batched and Cowles dissolved under a nitrogen blanket. The density measurements were made on the first and second cut of this submix for Batches 1 and 2. Since frothing does occur, the first cut is always less dense than the second. The density of the binder varies with the standing time after Cowles dissolving. Table 15 indicates the extent of this change. These data indicate that in less than 4 hr the frothing or foaming has broken and the density has increased to a value that is stationary for at least 24 hr. Although small gas bubbles can still be seen in the binder, the liquid density (within the limit of accuracy of this liquid density measurement) is close to that of the degassed binder. This shows that the Cowles dissolving method of introducing gas bubbles will be highly time dependent. Also, the liquid density of the aerated binder is dependent upon the procedure for Cowles dissolving. However, a fairly precise liquid density may be achieved in the aerated binder, and propellant batches were prepared with liquid densities from 0.8406 to 0.9260 gm/ml.

Table 15. Effect of Standing Time on Density of Aerated ANB-3226 Binder.

Sample Number	Density Immediately After Cowles Dissolving (gm/ml)	Density at Various Times After Cowles Dissolving (hr)			
		4	8	19	24
1	0.8777	0.9255	-	-	0.9260
2	0.8740	-	0.9298	0.9298	-
3	0.8784	-	0.9333	0.9333	-

In addition to the study of Cowles dissolve aeration, it was thought that mixing and casting techniques should be studied. The following test plan was used.

Batch Number	Liquid Density of Binder (gm/ml)	Change in Mixing and Casting Technique
1	0.8515	None; low density binder
2	0.9260	None; high density binder
3	0.8475	None; control for new submix
4	0.9145*	Same as No. 3 except Al is added with DER to submix to increase viscosity; decrease foam
5	0.8406	Same as No. 4 except a new submix and new day of mixing is involved (Control)
6	0.8556	Same as No. 5 except vacuum casting

*Unable to achieve low density binder by Cowles dissolving because of too small an amount of submix left for this batch.

REFERENCES

1. Project SOPHY - Solid Propellant Hazards Program, Technical Documentary Report AFRPL - TR - 66-25, Aerojet Report 0977-01 (03)QP (28 June 1966).

2. Large Solid-Propellant Boosters Explosive Hazards Study Program (Project SOPHY), Technical Docmentary Report AFRPL-TR-65-211, Aerojet Report 0866-01(01)FP (24 November 1965).

3. Project SOPHY - Solid Propellant Hazards Program, Technical Documentary Report AFRPL-TR-66-24, Aerojet Report 0977-01(02)QP (24 March 1966).

4. The Design and Analysis of Sensitivity Experiments, Rocketdyne Report R-6152 (May 1965).

5. Dixon, W. J., "Analysis of Extreme Values," Annals of Mathematical Statistics, Vol. 21, 488-506 (1950).

6. Cook, M. A., The Science of High Explosives, American Chemical Society Monograph Series, Reinhold Publishing Company, New York, N. Y., pp 144f (1958).

7. Liddiard, T. P., Jr., "The Initiation of Burning in High Explosives by Shockwaves," The Fourth Symposium on Detonation, Preprints, Vol. II, C-109f (1965).

8. Gibson, F. C., M. L. Bowser, and C. M. Mason, "Method for the Study of Deflagration to Detonation Transition," Rev. Sci. Inst., Vol. 30, No. 10, 916-919 (October 1959).

9. Jaffe, I., and D. Price, Progress Report on Adaption of Continous Wire Method for Measuring Transient Phenomena, NOLTR-63-136. U.S. Naval Ordnance Laboratory, White Oak, Md. (7 June 1963).

10. Price, D., I. Jaffe, and J. P. Toscano, Development of the Continuous Wire Method, Progress Report II, NOLTR 66-21, U.S. Naval Ordnance Laboratory, White Oak, Md. (17 March 1966).

REFERENCES (Continued)

11. 22-Inch Critical-Diameter Tests of Minuteman Stage II, Wing VI Propellant. Aerojet-General Corporation Final Report 0713-53-511, Contract AF04(694)258, CCN 28 (20 March 1964).

12. Analysis of Shock Attenuation for 0.5- and 2.0-in. Diameter Card-Gap Sensitivity Tests, Aerojet-General Corporation Special Report SRP 289 (20 January 1962).

DISTRIBUTION

AFRPL (RPMX)
Edwards, Calif. 93523 (10)

AFETR (MTDRD-4)
Patrick AFB, Florida 32925
Attn: Mr. G. Galfo (2)

AFETR (MTORS-3)
Patrick AFB, Florida 32925
Attn: Mr. L. J. Ullian (2)

NASA, Lewis Research Center
Chemical Propulsion Division
Cleveland, Ohio
Attn: Mr. J. J. Kramer (1)

NASA-MSFC
R-P & VE
Huntsville, Alabama
Attn: Mr. A. L. Wheeler (1)

Armed Services Explosive
Safety Board
Room 2075, T-7 Bldg.,
Gravelly Pt
Washington, D. C. 20315
Attn: Technical Office (2)

NASA, Langley Research
Langley, Virginia
Attn: Mr. R. Swain (1)

Rohm & Haas Chemical Co.
Redstone Arsenal
Huntsville, Alabama
Attn: Dr. H. Shuey (1)

NASA/MSFC
R-P & VE - MCP
Huntsville, Alabama
Attn: Dr. J. B. Gayle (1)

Aerospace Corporation
P.O. Box 95085
Los Angeles, California
Attn: Reports Acquisition Branch (1)

NASA Headquarters
600 Independence Ave.
Washington, D. C.
Attn: Mr. W. Cohen (1)

Defense Supply Agency
Defense Contract Admin. Services
11099 South La Cienega Blvd.
Los Angeles, California 90045
Attn: D. Ballain, ACO (1)

Headquarters
Air Force Flight Test Center
Air Force Systems Command
Edwards AFB, California
Attn: Mrs. M. Racovich
(FTMKR-4) (1)

Commander
Naval Ordnance Test Station
China Lake, California
Attn: Mr. F. Weals 3012 (1)

BSD (AFIAS-G2)
Norton AFB, California 92400 (2)

USAF (AFRSTD)
Washington, D. C. 20546
Attn: Mr. J. Johnson (1)

AFSC (SCIZM)
Andrews AFB, Wash., D. C.
20331
Attn: Mr. H. Ackerman (1)

BLANK PAGE

UNCLASSIFIED

Security Classification

DOCUMENT CONTROL DATA - R&D

(Security classification of title, body of abstract and indexing annotation must be entered when the overall report is classified)

1. ORIGINATING ACTIVITY (Corporate author)

Aerojet-General Corporation
Downey, California

2a. REPORT SECURITY CLASSIFICATION

Unclassified

2b. GROUP N/A

3. REPORT TITLE

Project SOPHY - Solid Propellant Hazards Program

4. DESCRIPTIVE NOTES (Type of report and inclusive dates)

Progress Report, 1 June - 31 August 1966

5. AUTHOR(S) (Last name, first name, initial)

Elwell, R. B.
Irwin, O. R.
Vail, R. W., Jr.

6. REPORT DATE	7a. TOTAL NO. OF PAGES	7b. NO. OF REFS
September 1966	93	12

8a. CONTRACT OR GRANT NO.	9a. ORIGINATOR'S REPORT NUMBER(S)
AF04(611)10919	
b. PROJECT NO. 623A00201	0977-01(04)QP
c.	9b. OTHER REPORT NO(S) (Any other numbers that may be assigned this report)
d.	AFRPL-TR-66-26

10. AVAILABILITY/LIMITATION NOTICES

Qualified requestors may obtain copies of this report from DDC.

11. SUPPLEMENTARY NOTES	12. SPONSORING MILITARY ACTIVITY
	AFRPL, Hazards Analysis Branch, AF Systems Command, Edwards AFB, Edwards, California

13. ABSTRACT

The critical diameter of 9.2% RDX-adulterated AP-PBAN propellant has been determined from the results of extensive testing. The critical dimension of a square cross-section column of the same material was found to be 7% smaller than the critical diameter. Data has been gathered from which an assessment of the applicability of a Jones-type detonation model to solid propellant will be made. The critical-diameter test of an unadulterated propellant (ANB-3226) at 60-in. diameter resulted in failure to sustain detonation. Results of this test are presented. Progress is reported in the synthesis of propellant that containe uniform distribution of small unconnected pores.

DD FORM 1 JAN 64 1473

UNCLASSIFIED

Security Classification

UNCLASSIFIED
Security Classification

14. KEY WORDS	LINK A		LINK B		LINK C	
	ROLE	WT	ROLE	WT	ROLE	WT
Propellant Hazards Critical Diameter Critical Geometry SOPHY Sensitivity						

INSTRUCTIONS

1. ORIGINATING ACTIVITY: Enter the name and address of the contractor, subcontractor, grantee, Department of Defense activity or other organization *(corporate author)* issuing the report.

2a. REPORT SECURITY CLASSIFICATION: Enter the overall security classification of the report. Indicate whether "Restricted Data" is included. Marking is to be in accordance with appropriate security regulations.

2b. GROUP: Automatic downgrading is specified in DoD Directive 5200.10 and Armed Forces Industrial Manual. Enter the group number. Also, when applicable, show that optional markings have been used for Group 3 and Group 4 as authorized.

3. REPORT TITLE: Enter the complete report title in all capital letters. Titles in all cases should be unclassified. If a meaningful title cannot be selected without classification, show title classification in all capitals in parenthesis immediately following the title.

4. DESCRIPTIVE NOTES: If appropriate, enter the type of report, e.g., interim, progress, summary, annual, or final. Give the inclusive dates when a specific reporting period is covered.

5. AUTHOR(S): Enter the name(s) of author(s) as shown on or in the report. Enter last name, first name, middle initial. If military, show rank and branch of service. The name of the principal author is an absolute minimum requirement.

6. REPORT DATE: Enter the date of the report as day, month, year; or month, year. If more than one date appears on the report, use date of publication.

7a. TOTAL NUMBER OF PAGES: The total page count should follow normal pagination procedures, i.e., enter the number of pages containing information.

7b. NUMBER OF REFERENCES: Enter the total number of references cited in the report.

8a. CONTRACT OR GRANT NUMBER: If appropriate, enter the applicable number of the contract or grant under which the report was written.

8b, 8c, & 8d. PROJECT NUMBER: Enter the appropriate military department identification, such as project number, subproject number, system numbers, task number, etc.

9a. ORIGINATOR'S REPORT NUMBER(S): Enter the official report number by which the document will be identified and controlled by the originating activity. This number must be unique to this report.

9b. OTHER REPORT NUMBER(S): If the report has been assigned any other report numbers *(either by the originator or by the sponsor)*, also enter this number(s).

10. AVAILABILITY/LIMITATION NOTICES: Enter any limitations on further dissemination of the report, other than those imposed by security classification, using standard statements such as:

(1) "Qualified requesters may obtain copies of this report from DDC."

(2) "Foreign announcement and dissemination of this report by DDC is not authorized."

(3) "U. S. Government agencies may obtain copies of this report directly from DDC. Other qualified DDC users shall request through _____."

(4) "U. S. military agencies may obtain copies of this report directly from DDC. Other qualified users shall request through _____."

(5) "All distribution of this report is controlled. Qualified DDC users shall request through _____."

If the report has been furnished to the Office of Technical Services, Department of Commerce, for sale to the public, indicate this fact and enter the price, if known.

11. SUPPLEMENTARY NOTES: Use for additional explanatory notes.

12. SPONSORING MILITARY ACTIVITY: Enter the name of the departmental project office or laboratory sponsoring *(paying for)* the research and development. Include address.

13. ABSTRACT: Enter an abstract giving a brief and factual summary of the document indicative of the report, even though it may also appear elsewhere in the body of the technical report. If additional space is required, a continuation sheet shall be attached.

It is highly desirable that the abstract of classified reports be unclassified. Each paragraph of the abstract shall end with an indication of the military security classification of the information in the paragraph, represented as *(TS)*, *(S)*, *(C)*, or *(U)*.

There is no limitation on the length of the abstract. However, the suggested length is from 150 to 225 words.

14. KEY WORDS: Key words are technically meaningful terms or short phrases that characterize a report and may be used as index entries for cataloging the report. Key words must be selected so that no security classification is required. Identifiers, such as equipment model designation, trade name, military project code name, geographic location, may be used as key words but will be followed by an indication of technical context. The assignment of links, rules, and weights is optional.

UNCLASSIFIED
Security Classification